



## The Mesoarchaean Akia terrane, West Greenland, revisited: New insights based on spatial integration of geophysics, field observation, geochemistry and geochronology

Agnete Steenfelt<sup>a,\*</sup>, Julie Hollis<sup>b</sup>, Christopher L. Kirkland<sup>c</sup>, Alessandro Sandrin<sup>a</sup>, Nicholas J. Gardiner<sup>c,f</sup>, Hugo K. H. Olierook<sup>c</sup>, Kristoffer Szilas<sup>d</sup>, Pedro Waterton<sup>d</sup>, Chris Yakymchuk<sup>e</sup>

<sup>a</sup> The Geological Survey of Denmark and Greenland, Øster Voldgade 10, 1350 Copenhagen K, Denmark

<sup>b</sup> Geology Department, Ministry of Mineral Resources, Government of Greenland, P.O. Box 930, 3900 Nuuk, Greenland

<sup>c</sup> Centre for Exploration Targeting – Curtin Node, The Institute for Geoscience Research, John de Laeter Centre, School of Earth and Planetary Sciences, Curtin University, Perth, Western Australia 6102, Australia

<sup>d</sup> Department of Geosciences and Natural Resource Management, University of Copenhagen, Øster Voldgade 10, 1350 Copenhagen K, Denmark

<sup>e</sup> Department of Earth and Environmental Sciences, University of Waterloo, Waterloo, Ontario N2L 3G1, Canada

<sup>f</sup> School of Earth and Environmental Sciences, University of St. Andrews, St. Andrews KT16 9AL, United Kingdom

### ARTICLE INFO

#### Keywords:

Mesoarchean crust  
Diorite  
TTG  
Aeromagnetometry  
North Atlantic Craton  
Akia terrane

### ABSTRACT

The northern part of the North Atlantic Craton (NAC) in southern West Greenland comprises a large tract of exposed Meso-Neoarchaean continental crust, divided into the ca 3300–2900 Ma Akia and ca 2900–2500 Ma Tuno terranes. We combine aeromagnetic, stream sediment geochemical, new litho-chemical and zircon geochronological data with previously published data to re-evaluate the crustal architecture and evolution of the Akia terrane and its boundary towards the Tuno terrane.

The previously recognised, but overlooked, Alanngua complex, situated between the Akia and Tuno terranes is bounded by aeromagnetic lineaments interpreted as Neoarchaean shear zones and has a distinct spectrum of Neoarchaean magmatic and metamorphic zircon ages that are rare in the Akia terrane. The Alanngua complex comprises components derived from both the Akia and Tuno terranes and is interpreted as a tectonic melange created during the Neoarchaean assembly of the NAC.

Within the Akia terrane, the chemistry of orthogneiss samples indicate that a large percentage is too mafic to classify as TTG s.s., implying that not only partial melting of mafic crust, but also some yet unaddressed mantle involvement is necessary in their formation. Previous models for the generation of the ca. 3015–2990 Ma quartz-dioritic Finnefjeld and Tasersuaq complexes conflict with their geochemical variation. We argue that the complexes may be genetically linked to buried gabbro-dioritic rocks indicated by their strong aeromagnetic response. Formed at same time are carbonatite, high-Mg gabbro and tonalite-trondhjemite, and we propose that this wide spectrum of rocks was formed by lithospheric and crustal melting in response to asthenospheric upwelling possibly in an extensional setting.

Periods of extensive magmatism in the Akia terrane were previously recognised at ca. 3220–3180 Ma and 3070–2970 Ma. We now subdivide the latter period into three episodes: juvenile basaltic-andesitic volcanism at 3070–3050 Ma; tonalitic and dioritic plutonism at 3050–3020 Ma, and gabbroic-dioritic plus tonalitic-trondhjemitic plutonism at 3020–2985 Ma. This last episode was immediately followed by crustal reworking during collision at 2980–2950 Ma.

\* Corresponding author.

E-mail address: [agnete.steenfelt@gmail.com](mailto:agnete.steenfelt@gmail.com) (A. Steenfelt).

<https://doi.org/10.1016/j.precamres.2020.105958>

Received 12 September 2019; Received in revised form 1 June 2020; Accepted 7 October 2020

Available online 15 October 2020

0301-9268/© 2020 The Authors.

Published by Elsevier B.V. This is an open access article under the CC BY-NC-ND license

(<http://creativecommons.org/licenses/by-nc-nd/4.0/>).

## 1. Introduction

The Mesoarchaean witnessed a period of major crust-building when planetary geodynamics may have shifted from a dominant vertical to a dominant horizontal tectonic regime (e.g. reviews by Arndt, 2013; Hawkesworth et al., 2017; Brown et al., 2020; Palin et al., 2020). Studies of Mesoarchaean crust are therefore crucial to increase the knowledge about crustal formation and reworking at that time. In this paper we address the northern part of the Archaean North Atlantic Craton (NAC) in southern West Greenland, which includes a well-exposed section ca. 170 by 100 km of Mesoarchaean crust, the Akia terrane (Fig. 1A). The NAC extends from Canada via southern Greenland to the Lewisian of northern Scotland and is one of the key examples of early Archaean cratons (Bridgwater et al., 1974; Friend et al., 1988; Friend and Nutman, 2019). In West Greenland, the NAC comprises felsic to intermediate orthogneiss intercalated with remnants of supracrustal belts and mafic to ultramafic and anorthositic plutonic rocks (reviews by Henriksen et al., 2000; Windley and Garde, 2009; Polat et al., 2015). The NAC crust was built over the period 3800 to 2500 Ma through assembly of a number of distinct tectono-stratigraphic terranes (Friend et al., 1988; Nutman et al., 2004; Polat et al., 2015; Gardiner et al., 2020).

The Mesoarchaean 3220–2970 Ma Akia terrane was defined as a crustal entity by Friend et al. (1988), when its southern boundary with an assemblage of Eo- to Neoarchaean terranes around Nuup Kangerlua (previously known as Godthaabsfjord) was established (Friend and Nutman, 2019, and references therein). Neoarchaean metamorphic and magmatic ages of rocks north of the Akia terrane indicated the presence

of another terrane which was termed the Tuno terrane (Friend and Nutman, 1994; Nutman et al., 2004; Garde et al., 2000). However, the exact location and nature of the boundary between the Akia and Tuno terranes in this poorly investigated part of the NAC are not well established.

Following early reconnaissance work along the West Greenland coast, Noe-Nyegaard and Ramberg (1961, before the terrane concept), recognised a number of discrete crustal complexes based on lithological assemblages, metamorphic grade and deformation style. One of these, the Alanngua complex is situated in the boundary region between the Akia and Tuno terranes (Fig. 1A), however, its existence has been overlooked by more recent papers discussing the Akia–Tuno boundary (Garde et al., 2000; Nutman et al., 2004; Windley and Garde, 2009; Yi et al., 2014; Dyck et al., 2015; Kirkland et al., 2018).

Most of the geological research in the Akia terrane has been concerned with the southern and eastern part of the terrane (Garde, 1997, 2007; Garde et al., 2000; Szilas et al., 2015, 2017). Field visits, zircon geochronology, petrology and geochemistry at selected localities within and surrounding the Finnefeld complex (Fig. 1) were conducted in search of evidence for a  $\geq 3$  Ga old giant meteoritic impact (Garde et al., 2012a; 2014; Keulen et al. 2015; Scherstén and Garde, 2013). Otherwise, geological information from the northern and north-western part of the Akia terrane has been scarce until 2016, when the Ministry of Mineral Resources (MMR) initiated investigations for the production of a new Maniitsoq map sheet (Fig. 1). This research involved new field work and collection of many samples for litho-geochemistry, geochronology and petrology. Based on the new data, a number of publications

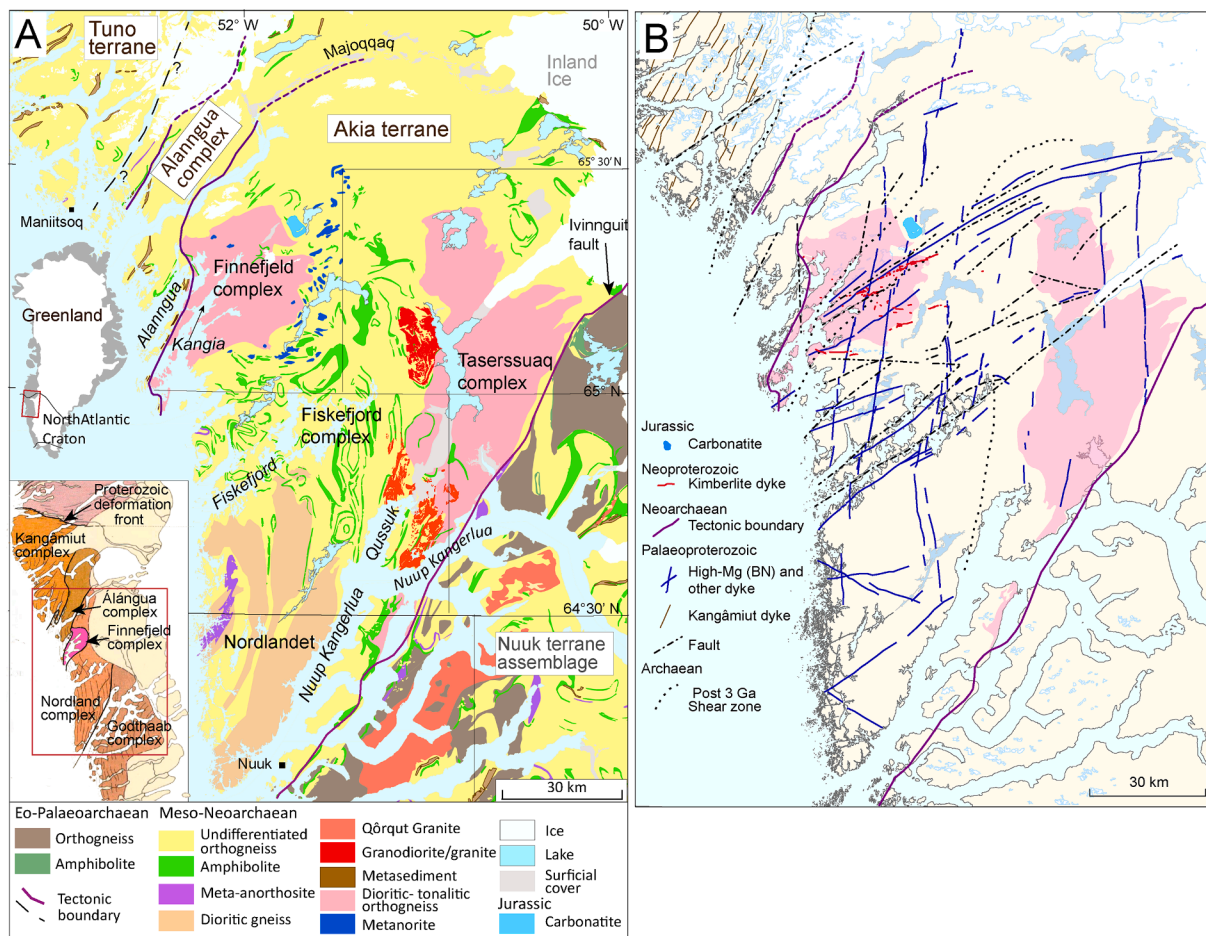


**Fig. 1.** A Main lithological units within the Nuuk-Maniitsoq region based on geological mapping by the Geological Survey of Greenland (references in text) and Friend and Nutman (2019). Frames for published geological map sheets at scale 1:100,000. Lower inset map modified from Noe-Nygaard and Ramberg (1961). B. Archaean shear zones and post-Archaean dykes and faults.

have addressed aspects of the crustal evolution and geodynamic setting of the Akia terrane (Kirkland et al., 2018; 2020; Gardiner et al., 2019, 2020; Yakymchuk et al., 2020; Olierook et al., 2020). As this new data is largely restricted to the northern part of the Akia terrane, it is uncertain if the proposed geodynamic implications of these new observations are valid across the entire terrane. For example, orthogneiss ages in the northern part of the Akia terrane are somewhat younger than those determined in the southern part of the Akia terrane (Garde, 2007; Gardiner et al., 2019), and other potentially significant differences between the northern and southern parts of the terrane has not been examined. Likewise, the genesis of the 3015–2990 Ma Finnefjeld and Taserssuaq orthogneiss complexes is uncertain.

In order to deal with these issues, we have integrated available data from aeromagnetometry and stream sediment geochemistry together with available reported field observations, lithological, rock geochemical and geochronological data for the entire Akia terrane and its northern boundary region, and studied their spatial variations relating to crustal architecture, composition and evolution.

In this paper, we demonstrate that the Alanngua complex is a distinct crustal segment with a separate Neoarchean history that is not shared by the Akia terrane. We present evidence that the Akia terrane hosts a significant proportion of dioritic gneiss in addition to tonalitic-trondhjemitic-granodioritic (TTG) gneiss, with the implication that mantle involvement is required for the generation of the Mesoarchean crust exposed in this part of the NAC, at least to a higher degree than assumed for Archaean crust elsewhere (e.g. Moyan and Martin 2012, Halla et al., 2017). Furthermore, we chronicle chemical and chronological diversity within the Akia Terrane and propose that the protoliths to the Finnefjeld and Taserssuaq complexes may be linked to a large subsurface gabbro-dioritic complex indicated in aeromagnetic data. Within the Mesoarchean evolution of the Akia terrane we recognise four distinct episodes of magma formation and metamorphism in the period 3300–2900 Ma, each with discrete extent and magma compositions.

## 2. Regional geology

### 2.1. The Akia terrane

The south-eastern Akia Terrane along Nuup Kangerlua (formerly Godthaabsfjord) encompasses a zone with amphibolite-facies rocks, orthogneisses and mafic to intermediate metavolcanic rocks, as well as prominent ultramafic bodies, that bounds against granulite-facies orthogneisses of Nordlandet to the west and the Ivinnugit fault to the east (Fig. 1; McGregor, 1993; Garde, 1997, 2007; Hollis et al., 2006).

Nordlandet (Fig. 1A) hosts the oldest part of the Akia Terrane – 3230–3190 Ma old dioritic orthogneisses (Garde, 1997) and migmatites with ca 3250 Ma xenocrystic zircons (Naeraa et al., 2012; Gardiner et al., 2019). The Nordlandet metadiorites were intruded by 3050 Ma tonalites (Garde, 1997).

The Fiskefjord complex occupies the south-central part of the Akia Terrane around Fiskefjord. The complex consists of felsic to intermediate orthogneisses interleaved with mafic metavolcanic rocks and their associated bodies of metagabbro to metaperidotite, some of which are layered igneous complexes (Nutman et al., 1989; Garde 1987, 1997; Garde et al., 2000; Szilas et al., 2015; Aarestrup et al., 2020). The Fiskefjord complex was formed, metamorphosed at granulite-grade conditions and variably retrogressed at amphibolite-grade within the age range 3070–2970 Ma (McGregor, 1993; Garde et al., 2000). Geodynamically, the Fiskefjord complex has been described as a convergent plate tectonic setting where metavolcanic sequences along Nuup Kangerlua-Qussuk (Fig. 1) represent remnants of a volcanic arc and the orthogneiss of the Fiskefjord complex represent tonalite and diorite generated during subduction (Garde 2007, Szilas et al., 2017). However, mantle involvement was required for the generation of the Qeqertausaq metadiorite with sanukitoid-like composition (Steenfelt et al., 2005a).

The orthogneiss-amphibolite assemblage appears to continue northwards, where it is intruded by the Finnefjeld and Taserssuaq complexes.

The eastern part of the Fiskefjord complex is at lower metamorphic grade and the orthogneiss-amphibolite assemblage contains late, granodioritic to granitic (ca 2975 Ma) dome-like granitoids (Fig. 1A) within a zone dominated by upright folds with strong N–S elongations bordering the Taserssuaq complex (Garde, 1997; Garde et al., 2000). This late magmatism was interpreted to represent crustal melting during craton stabilisation (Garde, 2007).

The N–S trending 3013–3001 Ma Maniitsoq Norite belt comprises abundant bodies of orthopyroxene-bearing, high-Mg meta-norites and -gabbro-norites (6–26% MgO, high Cr and Ni) forming steep to shallow sheet-like intrusions from a few metres up to 4 km in size (Secher, 1983; Waterton et al., in review). Several of the bodies host Ni-Cu-Co(-PGE)-sulphide mineralisation with economic potential. Small high-Mg-Cr-Ni metadiorite plugs intrusive into the Fiskefjord complex (Garde, 1991; Garde et al., 2000) have been correlated with the metanorites (Garde et al., 2012b). The metanorite bodies show post-intrusion ductile deformation, shearing and faulting (Ravenelle and Weiershäuser, 2017; Waterton et al., 2020).

The northern part of the Akia Terrane features undifferentiated granulite and amphibolite-facies orthogneisses containing remnants of mafic supracrustal rocks (Allaart, 1982; Kalsbeek and Garde, 1989). The rock assemblage thereby resembles the Fiskefjord complex, but orthogneiss ages are younger ca. 3020–2990 Ma (Scherstén and Garde, 2013; Gardiner et al., 2019). The small (500 by 200 m), 3007 ± 2 Ma Tupertalik carbonatite intrusion occurs in this part of the Akia Terrane (Larsen and Pedersen, 1982; Bizzarro et al., 2002).

The Finnefjeld complex (previously known as Finnefjeld gneiss) was first described as a homogeneous, metamorphic, hornblende-bearing, quartz-dioritic unit which has intruded into the Fiskefjord complex and has enclaves of folded metavolcanic rocks at the margins (Noe-Nygaard and Ramberg, 1961; Berthelsen, 1962; Allaart, 1982). The predominant felsic quartz-dioritic to granodioritic component of the Finnefjeld gneiss hosts variably digested inclusions of diorites (presumed cognate) as well as components of tonalitic to granodioritic composition, and it is best described as a multiphase intrusive complex with a composition varying from diorite to granite (Gardiner et al., 2019). The Finnefjeld complex has been affected by strong post-intrusive ductile deformation with development of NE to NNE steep foliation (Berthelsen, 1962; Allaart, 1982), some of which may be Neoarchean in age (Kirkland et al., 2018). Additionally, Palaeoproterozoic, Neoproterozoic and Mesozoic brittle deformation has affected the area (Fig. 1B). The Finnefjeld complex has been regarded a late magmatic product of the Fiskefjord complex (Garde, 1997) in accord with a zircon U-Pb age of 2975 ± 7 Ma (Garde et al., 2000). More recently, the complex and surroundings were interpreted as a giant ca 3000 Myr old meteoritic impact structure and the originally determined age of the Finnefjeld gneiss was reinterpreted as having been affected by isotopic resetting (Garde et al., 2014 and references therein, Scherstén and Garde, 2013). The impact hypothesis, however, has been questioned (Reimold et al., 2013, Kirkland et al., 2018, Gardiner et al., 2019; Reimold et al., 2014) and is also at odds with the aeromagnetic, geochemical and geochronological data presented and discussed in the present study. Gardiner et al. (2019) obtained 3011–2994 Ma zircon ages for the Finnefjeld complex and suggested that the coeval generation of the Finnefjeld Complex and surrounding orthogneiss was accomplished by melting of mafic crust over a substantial lithospheric depth.

The large Taserssuaq complex (Taserssuaq granodiorite or tonalite in previous literature) orthogneiss complex showing compositional variation from diorite to tonalite and granodiorite similar to the Finnefjeld complex, and likewise intrusive into the Fiskefjord complex. The Taserssuaq complex locally exhibits magmatic layering and has inclusions of dioritic and gabbroic gneiss, and the complex is weakly deformed in open folds (Allaart et al., 1978; Hall, 1984; Garde et al., 1983, 1986, 1997; Garde, 2007). The Taserssuaq and Finnefjeld

complexes are considered coeval and the original age of ca. 2982 Ma for the Taserssuaq complex (Garde et al., 1986) was interpreted as isotopic resetting by Scherstén and Garde, (2013), who obtained a zircon age of  $2995 \pm 3$  Ma for a sample from the Taserssuaq complex matching the ca. 2991 Ma age obtained by Hanmer et al. (2002).

Discordant, up to one metre wide irregular dykes of fine-grained grey metagranodiorite were emplaced at ca. 2970 Ma and are common both within and in the surroundings of the Finnefjeld and Taserssuaq complexes (Garde et al., 1983; Hall, 1984; Olierook et al., 2020) making them a marker of the extent of post Finnefjeld-Taserssuaq magmatism.

## 2.2. The Alannua complex and Tuno terrane

The Alannua complex comprises strongly folded tonalitic orthogneisses and a higher proportion of metasedimentary rocks than observed in the adjacent complexes. Biotite schists with garnet, sillimanite and kyanite occur along with various types of diopside-rich amphibolites, garnet amphibolite and amphibolitic schists (Noe-Nygaard and Ramberg, 1961). Lenticular enclaves of epidote-rich calc-silicate rocks are common and prominent ultramafic bodies are associated with the supracrustal rocks. Upon studies of the boundary zone between the Alannua and Finnefjeld complexes, it was concluded that the Finnefjeld complex, has been thrust in a north-westerly direction over the Alannua complex (Berthelsen, 1962). Orthogneiss has yielded ages of 3019–2990 Ma (Gardiner et al. 2019; Yakymchuk et al., 2020). Late Mesoproterozoic U-Pb ages of detrital zircons (ca 2880–2850 Ma) were interpreted as depositional ages for the metasedimentary rocks and metamorphic zircon ages 2700–2550 Ma were recorded in this area (Kirkland et al., 2018; Garde et al., 2000; Dyck et al., 2015).

To the north-west of the Alannua complex, the Tuno terrane is dominated by 2870–2700 Ma granulite-facies orthogneisses that continues northwards to and beyond the deformation front of the Palaeoproterozoic Nagssugtoqidian orogen (Fig. 1; Garde et al., 2000; Connelly and Mengel, 2000; van Gool et al., 2001). The southern boundary of the Tuno terrane has not been firmly established but is addressed in this study.

## 2.3. Post-Archaean events

Palaeoproterozoic crustal rifting across the NAC was accompanied by intrusion of doleritic dyke swarms and faulting (Nilsson et al., 2010; Nilsson et al., 2013). In the study region (Fig. 1B) older, ca 2210 Ma dykes (Nutman et al., 1995); are mostly N-S striking with a few striking NE (Berthelsen and Bridgwater, 1960; Berthelsen, 1962). They have a distinctive geochemical signature of high MgO (ca 16%), Cr and Ni contents paired with relatively high SiO<sub>2</sub>, light rare-earth and large ion lithophile element concentrations and are termed boninite-norite dykes (BN dykes; Hall and Hughes, 1987). Younger NNE-striking Kangamiut dykes (Fig. 1B) are the southernmost extent of a swarm of tholeiitic dolerites (ca 2040 Ma; Nutman et al., 1999; Mayborn and Lesher, 2006). Both types of mafic dykes are up to and occasionally beyond 100 m in width and many can be traced for several tens of kilometres along strike.

The Fiskefjord faults are a system of NE-trending wrench faults that are seen in the central part of the region, where they off-set the BN dykes. The faults are accompanied by brecciation and other forms of brittle deformation and immediate surroundings of the faults contain greenschist-facies mineral assemblages (Berthelsen, 1962).

Kimberlite dykes belonging to the late Neoproterozoic (ca. 600–550 Ma) Sarfartoq-Maniitsoq alkaline province are typically 20–100 cm wide and occur in the northern part of the Akia Terrane (Nielsen et al., 2009; Tappe et al., 2011). The main zone of kimberlites trends NE and the dykes are emplaced en-echelon striking 080° within that zone (Fig. 1B). The kimberlites carry microdiamonds in sub-economic amounts (Steenfelt et al., 2009).

After intrusion of the kimberlites, no Phanerozoic tectonic or magmatic event is documented until the Jurassic when faulting and

intrusion of the Qaqarsuk carbonatite complex with associated ultramafic lamprophyres occurred at ca 160 Ma (Tappe et al., 2017). Ring-shaped massive carbonatite sheets are surrounded by a zone of fenitisation as well as a system of late dm-wide ferro-carbonatite dykes that can be traced far from the main carbonatite typically following existing NE trending fractures (Knudsen, 1991; Secher, 1983). An explosion breccia (Fossilik) embeds downfaulted blocks with Palaeozoic limestone (Poulsen, 1966; Stouge and Peel, 1979). The youngest magmatic rocks in the region are generally coast-parallel, typically <100 cm wide Palaeogene lamprophyre dykes and an alkali basalt plug recognised in the north-western part (Larsen et al., 2009).

## 3. Datasets and methods used

### 3.1. Aeromagnetic data

The Akia terrane is covered by the airborne survey Aeromag 1998, a fixed-wing magnetometer survey with 500 m spacing and 300 m ground clearance (Rasmussen and Thorning, 1999).

The analysis of the aeromagnetic data was performed in Geosoft®, and the map of total magnetic intensity (TMI) is presented as colour-contoured and shaded, grid-based images using the minimum curvature method of gridding and a grid size of 100 m (Fig. 2A; Rasmussen and Thorning, 1999). The software allows to extraction of various attribute maps used to enhance tectonic features and investigate the presence of highly magnetic rocks in the subsurface (e.g. Henkel, 1991, Airo, 2002; Sandrin and Elming, 2006; Sandrin et al., 2007). The tilt derivative attribute (Fig. 2B) is calculated from TMI data to improve the detection of shape and edge of the magnetic sources (Verduzco et al., 2004). The tilt derivative is defined as  $\tan^{-1}$  of the square root of the ratio between first vertical derivative and total horizontal derivatives of the TMI. The upward continuation of the TMI provides a simulation of the downward continuation of the magnetic field by removing the short-wave variation in the data (Jacobsen, 1987). The upward continuation is produced by Fourier transformation of the potential field data, multiplication of the transformed data by  $e^{-Kh}$ , where h is the height and K is the wavenumber, followed by an inverse Fourier transformation.

### 3.2. Stream sediment geochemistry

Chemical major and trace element data are analysed within the < 0.1 mm grain size fraction of systematically collected composite stream sediment samples at a density of 1 sample station per 20 to 50 km<sup>2</sup>. Sample stations are preferably situated in second or third order streams with catchment areas <20 km<sup>2</sup> in size (Steenfelt, 1987; Steenfelt, 2001, 2012; Steenfelt et al., 2005b). Analytical methods include X-ray fluorescence spectrometry, atomic absorption spectrometry and instrumental neutron activation. Analytical data from individual sample batches are quality controlled and corrected to eliminate analytical bias between methods and laboratories (Steenfelt, 1999).

Whereas the finest fraction of stream sediment was analysed for major and trace elements, the 0.25–1 mm grain size fraction of stream sediments from samples across the Archaean craton were processed to recover kimberlite indicator minerals (Steenfelt, 2001). The content (by weight) of magnetic minerals was recorded during sample processing.

### 3.3. Lithology

The south and east of the Akia Terrane is mapped at a scale of 1:100,000 (Fig. 1; McGregor, 1984; Garde, 1987, 1989; Chadwick and Coe, 1988). The north and northwest of the terrane are only covered by a reconnaissance map at the scale of 1:500,000 (Allaart, 1982). Comprehensive descriptions of rock types and their relations in the mapped areas are found in McGregor (1993), Hall and Hughes, 1982 and Garde (1997).

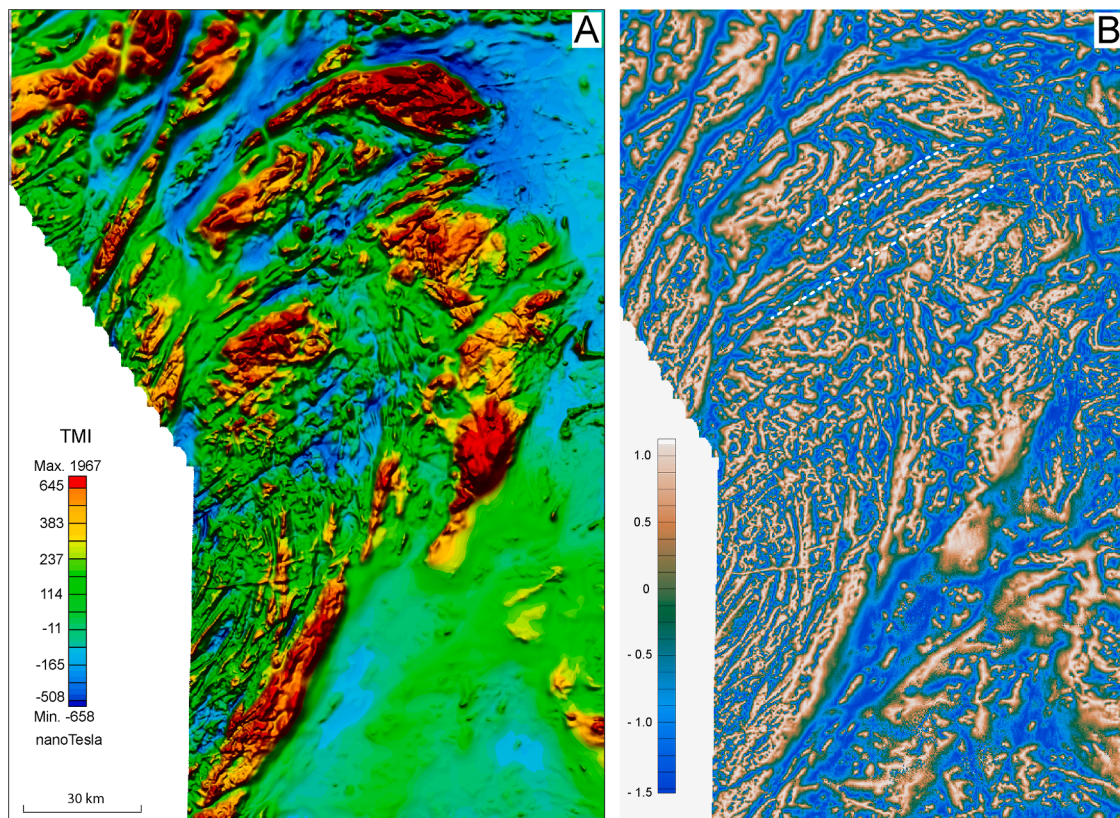


**Fig. 2.** Aeromagnetic maps of the Nuuk-Maniitsoq region based on Aeromag 1998 data (Rasmussen and Thorning, 1999). A: Total magnetic field intensity as colour-contoured shaded grid image. B: Tilt derivative attribute map obtained from TMI analysis. The tilt derivative enhances linear features and can be used to map subvertical contacts and faults. The dashed white lines outline the Kangia-Fossilik zone of Meso-Neoproterozoic ductile to post-Archaeozoic brittle deformation.

### 3.4. Whole rock geochemistry

New samples acquired by MMR had whole rock compositions determined at ALS Laboratories (Ireland). Major element concentrations were obtained using the ME-ICP06 analytical package, in which samples are analysed by ICP-AES following Li-metaborate fusion and acid digestion. Trace element concentrations were determined by ICP-MS following Li-metaborate fusion and acid digestion (ME-MS81 package) and following four-acid digestion (ME-MS61 package).

Archived data at The Geological Survey of Denmark and Greenland comprise whole rock compositions determined by X-Ray Fluorescence techniques for major and some trace elements, Instrumental Neutron Activation for other, see Garde (1997). The data used here are presented in Supplementary file S1.

### 3.5. Zircon U-Pb geochronology

#### 3.5.1. Shrimp

SIMS U-Pb analysis was performed on ten samples using Shrimp B in the John de Laeter Centre following analytical protocols matching those discussed in Wingate and Kirkland (2015). During the range of sessions these samples were analysed in, BR266 (Stern, 2001) was used as the primary reference material and at least ten analyses of this material were made interspersed with unknowns per session (Stern, 2001). Indicated external spot-to-spot (reproducibility) uncertainty was always better than 1% ( $1\sigma$ ), and  $^{238}\text{U}/^{206}\text{Pb}^*$  calibration uncertainty was always better than 0.5% ( $1\sigma$ ). Calibration uncertainties are included in the errors of  $^{238}\text{U}/^{206}\text{Pb}$  ratios and dates in Supplementary file S3. Analyses of the OG1 ( $3465.4 \pm 0.6$  Ma Stern, et al., 2009) standard yielded a  $^{207}\text{Pb}/^{206}\text{Pb}$  weighted mean age of  $3464 \pm 3$  Ma identical to the accepted value, and no  $^{207}\text{Pb}/^{206}\text{Pb}$  fractionation correction is deemed

necessary. Common-Pb corrections were applied to all SIMS analyses using contemporaneous isotopic compositions determined according to the Pb evolution model of Stacey and Kramers (1975).

#### 3.5.2. La-Icpms

Five samples were analysed for U-Pb by quadrupole LA-ICPMS. Zircon was ablated using a Resonetics RESOLUTION M-50A-LR system, incorporating a COMPex 102 193 nm excimer UV laser. Following a cleaning pulse and a 40 s period of background analysis, samples were spot ablated for 35 s at a 10 Hz repetition rate using a 50  $\mu\text{m}$  beam and laser energy at the sample surface of 2.0  $\text{J}/\text{cm}^2$ . An additional 40 s of baseline was collected after ablation. The sample cell was flushed with ultrahigh purity He (300 mL/min) and N<sub>2</sub> (1.0 mL/min) and high purity Ar was employed as the plasma carrier gas. Six U-Pb isotopes were measured using an Agilent 7700 s or 8900 quadrupole ICPMS, with high purity Ar as the plasma gas (flow rate 0.98  $\text{l min}^{-1}$ ). The dwell time on the mass stations was  $^{204}\text{Pb}$ ,  $^{206}\text{Pb}$ ,  $^{207}\text{Pb}$ ,  $^{208}\text{Pb}$  (0.03 s each),  $^{232}\text{Th}$  (0.0125 s), and  $^{238}\text{U}$  (0.0125 s). During time-resolved processing, contamination resulting from inclusions and compositional zoning was monitored, and only the relevant part of the signal was integrated. The primary reference material used for U-Pb dating in this study was zircon standard OG1 ( $3465.4 \pm 0.6$  Ma, Stern et al., 2009), which has an ablation response similar to the Archaeozoic grains of interest. Secondary standard zircon 91,500 ( $1062.4 \pm 0.4$  Ma; Wiedenbeck, et al., 1995), GJ-1 ( $601.7 \pm 1.4$  Ma; Jackson, et al., 2004), and Plešovice ( $337.13 \pm 0.37$  Ma; Sláma, et al., 2008) yielded  $^{206}\text{Pb}/^{238}\text{U}$  ages within 2% of the accepted value when reduced using appropriate matrix matched standards over the course of this study. The time-resolved mass spectra were reduced using the U/Pb Geochronology data reduction schemes in IoliteTM (Paton, et al., 2011), and in-house Microsoft Excel macros. No common lead corrections were deemed necessary due to generally low

$^{204}\text{Pb}$  counts. Those analyses with elevated  $^{204}\text{Pb}$  counts are not used in placing age constraints.

## 4. Results

### 4.1. Aeromagnetometry

The total magnetic field (TMI) for the region together with tilt-derivative of the magnetic field are shown in Fig. 2. The aeromagnetic survey coverage extends beyond the exposed land surface, i.e. the maps show the variation in magnetic parameters offshore, below lakes and perennial ice caps as well as below the margin of the Inland Ice.

Fig. 2 displays three major types of patterns: 1) coherent areas of high or low magnetic intensity with weak internal variation, 2) patterns of alternating magnetic highs and lows that reflect fold structures, and 3) magnetic lineaments, i.e. narrow high- or low-magnetic features that crosscut other features; these trace faults, shear zones and some dykes. The nature of the first type is enhanced by the upward continuation filtering (Fig. 3). The other two types are enhanced by the tilt derivative image (Fig. 2B). Magnetic highs and lows together with curved magnetic lineaments interpreted to trace shear zones are outlined and named in Fig. 4, and their relation to known lithology and structure is shortly described here and discussed in Section 5.2.

#### 4.1.1. Magnetic highs and lows

The aeromagnetic data shown here covers only a small part of the Tuno terrane, and they are not considered further. West of the Alanngua complex, a magnetic high (TK) is associated with orthogneiss of the shear zone bounded Tuno keel area, which, to the east, has a marked contrast to the low magnetic response from most of the Alanngua complex. The southern part of this complex has moderate response.

Within the Akia terrane, the Qullugiannguit (Q) and Isortoq (I) highs

dominate the northern part where outcropping granulite-facies orthogneiss and intervening slivers of mafic metavolcanic rocks prevail (Allaart et al., 1978). The low magnetic areas around and within the Isortoq high corresponds to areas of felsic orthogneiss. The largest and strongest magnetic high in the region (T) is clearly spatially associated with the Taserssuaq complex. The strongest magnetic intensity within this high occurs at its southern end, where a 5x5 km area with large bodies of metagabbro are enclosed by the Taserssuaq granodiorite (Fig. 4). A smaller high, Finne S (FS), is partly covered by the Finnefeld complex. The central part of the Finnefeld complex covers an area characterised by closely spaced NE trending lineaments, shear zones, dykes and faults, resulting in a pattern of parallel narrow highs and lows. This zone also hosts abundant brittle fractures and is termed the Kangia-Fossilik (K-F) zone. The northernmost part of the Finnefeld complex overlaps the southern fringe of the Isortoq high (Fig. 4).

The NNE-trending elongated Nordlandet East high (NE) follows the east coast of Nordlandet with the Qussuk high (QS) as a small extension to the north. The two highs are separated by the Qugssuk-Ulamertoq high-strain zone (Fig. 4; Garde, 1997). The upward continuation filtering indicates that the strongest aeromagnetic highs, Q, FS, T and NE are associated with long-wave magnetic anomalies with continuity to considerable depths (Fig. 3). Other highs, TK and I, appear associated with more shallow sources since they fade at simulated depths > 10 km (Fig. 3).

Low intensity in the total magnetic field is observed in the Four lakes and Nuup Kangerlua areas where they are associated with amphibolite-facies orthogneiss and mafic supracrustal rocks. These areas share the low magnetic response of the amphibolite-facies rocks prevailing in large areas of the Nuuk terrane assemblage.

#### 4.1.2. Fold patterns

Mafic metavolcanic rocks (amphibolite) interfolded with felsic orthogneiss are responsible for the fold pattern of magnetic highs and lows within the Fiskefjord complex (compare Fig. 2B with Fig. 4). Different folding styles and orientations in the northern and southern parts of the Akia terrane are observed. Complexly folded rocks in the south-western Fiskefjord complex overprinted by N-S oriented folds in the east and in eastern Nordlandet (Fig. 2B). The northern part of the Akia terrane exhibits large recumbent folds with NE to E axial trends.

#### 4.1.3. Faults

The aeromagnetic data highlight faults because magnetite destruction within epidote-greenschist facies margins along the faults causes a decrease in magnetic response (Henkel and Guzmán, 1977; Grant, 1985). Known faults in the study area are shown in Fig. 1B but omitted in Fig. 4, for clarity. In early mapping, faults were recognised only in the coastal areas. Aeromagnetic data have been used here to trace the faults further inland and to add a few in the northern area. The straight, NE-trending magnetic lineaments (Fig. 2 A, B) reflect the Fiskefjord fault system and coincide with topographic lineaments which may also track faults (Fig. 1B; Berthelsen and Bridgwater, 1960; Berthelsen, 1962). A remarkable shift in the orientation of faults is observed in the north-western part of the region, where the dominating NE-orientation across Akia is replaced by NNE-striking faults.

#### 4.1.4. Dykes

Moderately high magnetic linear NE-trending features can be shown to be spatially correlated with the wider of the high-Mg (BN) dykes. The magnetic signature is best seen on low-magnetic backgrounds, such as in the north-eastern part of Fig. 2B. Some of the N-S-striking dykes also induce weak traces in the TMI map, as do a few E-W-striking dykes in Nordlandet, but otherwise the dykes are not discernible at the scale of the figures shown here. The dykes shown in Fig. 1B are based on mapping assisted by aeromagnetic data.

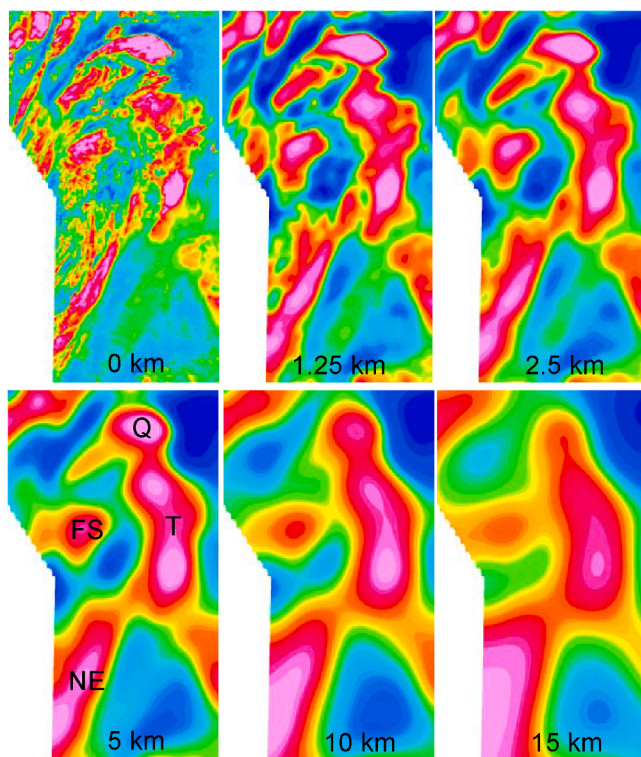
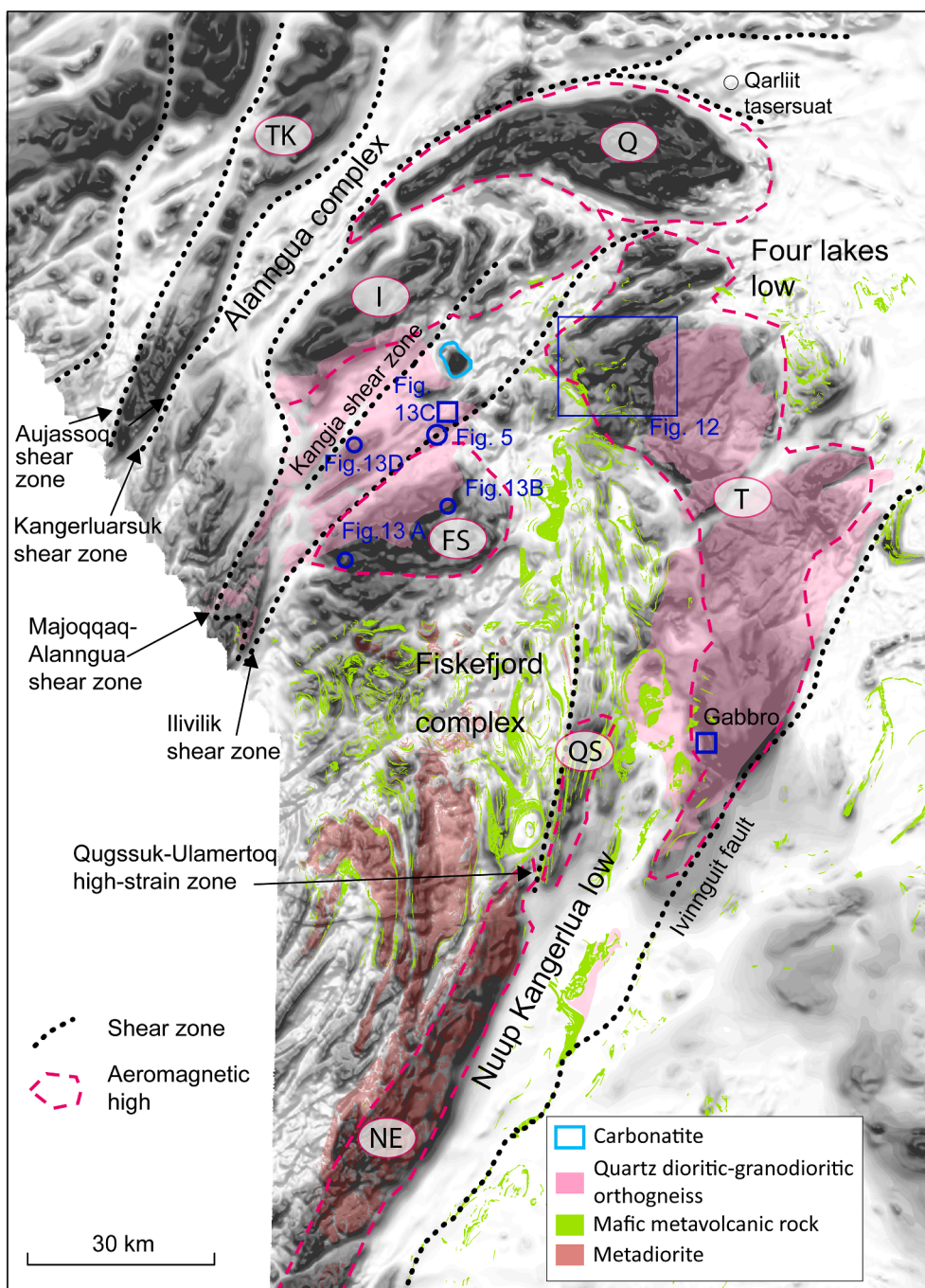


Fig. 3. Upwards continuation filtering of the total magnetic field in steps corresponding to depths from 0 to 15 km after Jacobsen (1987). The filter suppresses short-wave variation from near-surface sources thereby enhancing the long-wave variation assumed to be caused by subsurface structures. Downwards persistent features, Q, T, FS, NE, are shown and named in Fig. 4.



**Fig. 4.** Aeromagnetic data (TMI, grey-tone image) with superposed main lithological units from 1:100,000 scale maps (references in section 3.1) and positions of photos and map shown in later figures. Major magnetic lineaments interpreted as shear zones are marked and named. Areas of high and low magnetic intensity (magnetic highs and lows) are named: Tuno keel (TK), Qullugiannugit (Q), Isortoq (I), Taserssuaq (T), Finne S (FS), Qussuk QS, Nordlandet east (NE).

**4.1.5. Kangia-Fossilik zone (K-F zone).**

A ca.15 km wide NE-SW oriented zone dominated by NE-trending lineaments marking dykes, shear zones and faults cuts the northern Akia terrane and separates the northern magnetic highs from the Taserssuaq and Finnefeld S highs, best seen in the tilt derivative map (Fig. 2B). At its southwestern extent, the zone passes through the Finnefeld complex where steeply dipping, high strain foliations have the same orientation (Berthelsen, 1962). In the north-east, the K-F zone meets the Four Lakes low (see below), within which it is not recognisable as a distinct feature. The boundary truncates the northern Fiskefjord complex and the Taserssuaq complex, and the northern boundary is

parallel to the southern flank of the fold structure of the Isortoq high. Low magnetic bands are seen within the Isortoq high fold structure.

**4.1.6. Shear zones**

Hydrothermal alteration and weathering within and along shear zones reduce the magnetic susceptibility of the sheared rocks and make such zones appear as narrow linear magnetic lows (Henkel and Eriksson, 1987; Airo, 2002). It is characteristic that these lineaments are variably curved. Where they act as pattern-breaks, i.e. a shift in the shape or trend of magnetic variation patterns on either side, they are interpreted to track tectonic boundaries.



Fig. 5. Close-up of Ilivilik shear zone showing mylonitic texture at locality marked in Fig. 4 (65.3061 N, 51.5882 W). The SW-NE striking zone is here about 100 m wide with steep dip towards SE.

Four prominent lineaments are noted here and interpreted as shear zones, and for which we propose the following names (Fig. 4): Majoqqaq-Alanngua shear zone (along the Majoqqaq melt river to the fjord Alanngua, Fig. 1,4), Ilivilik, Kangerluarsuk and Kangia shear zones. The lineament on the western side of the Tuno keel high, the Aujassoq shear zone, is named and described as a belt of strong ductile shearing (Allaart and Jensen, 1979).

The Majoqqaq-Alanngua and Kangerluarsuk shear zones (Fig. 4), coincide with the northern and southern boundaries of the Alanngua complex as they are mapped in coastal areas by Noe-Nygaard and Ramberg (1961) and Berthelsen (1962). The inland continuation of the magnetic lineament along the Majoqqaq river likely traces the boundary between the Akia terrane and Alanngua complex. The Majoqqaq river has previously been regarded as the boundary between the Akia and Tuno terranes (Nutman et al., 2004) or between two Archaean blocks (Windley and Garde, 2009). In the easternmost end of the lineament a

bifurcation is indicated, which may correspond to terrane boundaries proposed by Yi et al. (2014).

The Ilivilik shear zone has not been previously recognised. Almost sinuous in shape, this strong magnetic lineament can be traced from the coast at the southern boundary of the Finnefeld complex, north-eastwards through this complex towards the north-eastern corner of the map (Fig. 2A and accentuated in Fig. 2B). A small part of the shear zone was observed during field work by the first author where it forms a ca. 100 m wide zone of shearing and mylonitisation (Fig. 5).

The Kangia shear zone was shown as a fault in Berthelsen and Bridgwater (1960). It lies between the Ilivilik and Majoqqaq-Alanngua shear zone where it follows the narrow Kangia fjord and seems to continue along the north side of the Qaqarsuk carbonatite (Fig. 4).

The southern part of the Ivinnuit fault, the boundary between the Akia and Nuuk terrane assemblage, is not visible in the magnetic map in its southern part, where there are low magnetic areas on either side. However, it is described as a tectonic break (McGregor et al., 1991) and appears similar to the other shear zones outlined in the TMI map (Fig. 4).

#### 4.2. Stream sediment geochemistry

Stream sediment samples in Greenland are largely composed of mineral grains because chemical weathering is very limited in the arctic climate. Therefore, the stream sediment chemistry can be used as a proxy for rock compositions (Steenfelt et al., 2005b) and will provide information on the character of the rocks in areas where rock samples are missing. Three components are chosen to illustrate properties of the exposed crust, the magnetic fraction, nickel and rubidium contents.

##### 4.2.1. Magnetic fraction

The aeromagnetic data result from both surface and subsurface sources, where the contribution from the latter depends on size, burial depth and magnetic susceptibility of the cover, e.g. solid rocks or surficial deposits. The magnetic fraction of stream sediment, i.e. the content of magnetic minerals (primarily magnetite and titanomagnetite), is indicative of the contents of these minerals in the exposed surrounding rocks and can therefore be used to verify if an aeromagnetic anomaly is caused by outcropping rocks. Low contents in stream sediment samples

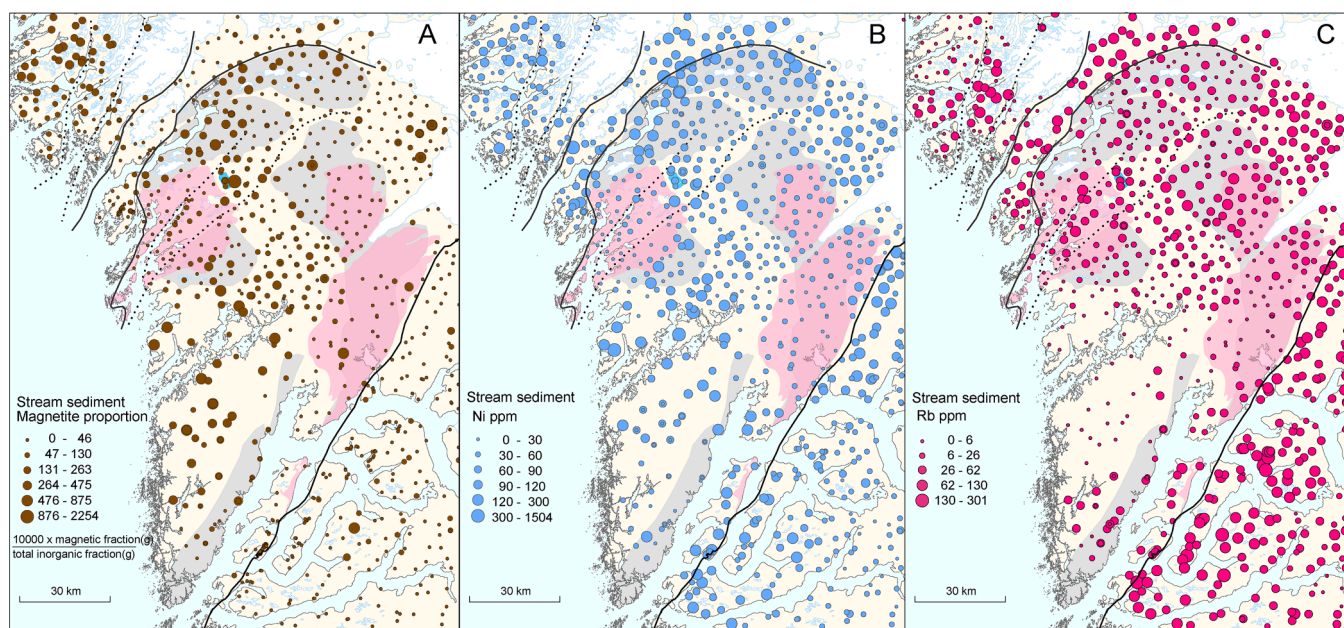
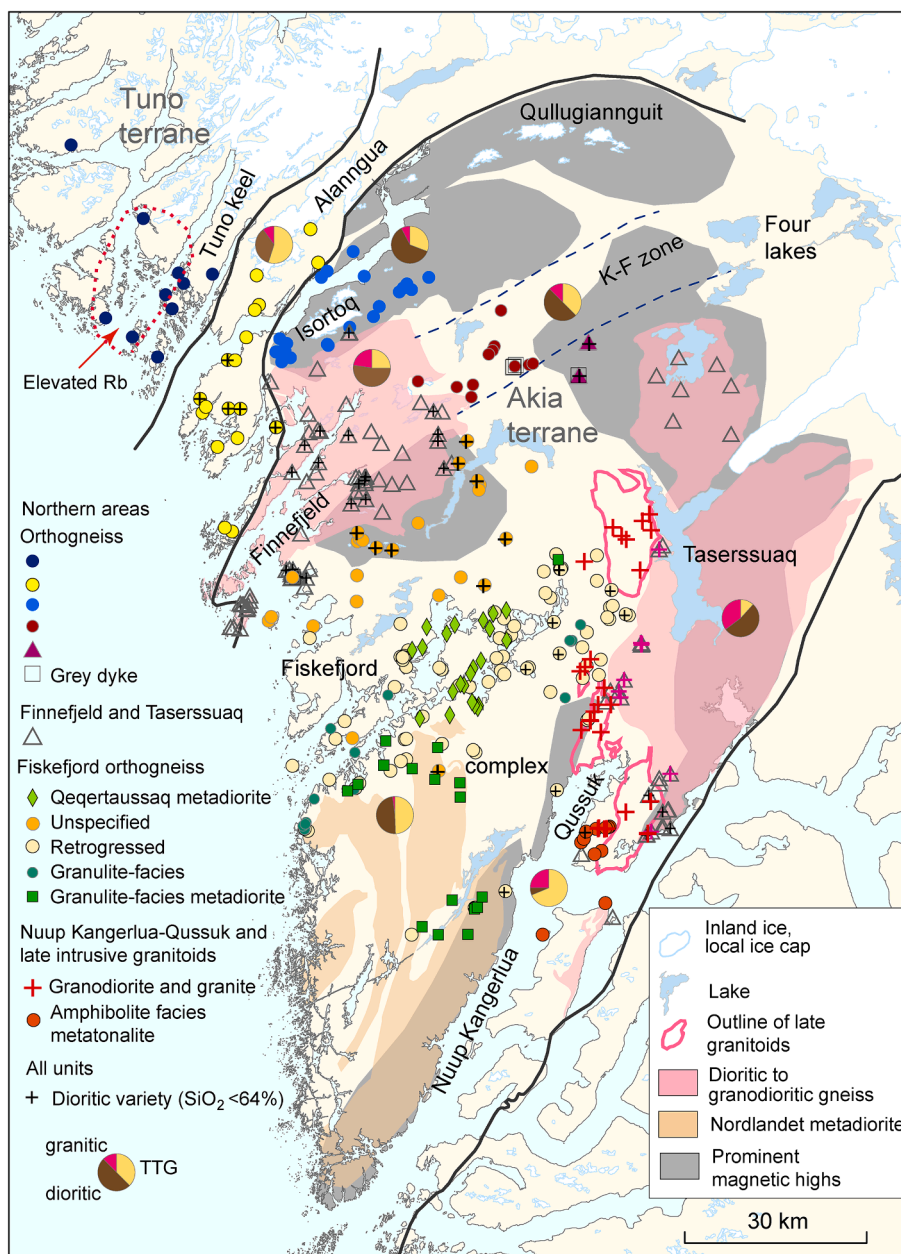


Fig. 6. Selected geochemical data based on systematically acquired stream sediment samples (Steenfelt 2001). A: Magnetic fraction of the 0.25 to 1 mm grain size fraction reflects the amount of magnetic minerals held by outcropping rocks. B and C: Concentration of nickel and rubidium, respectively, in the < 0.1 mm grain size fraction. Elevated to high Ni reflect occurrences of mafic to ultramafic rocks. Elevated to high Rb reflect granodioritic and granitic rocks.



**Fig. 7.** Location of 428 chemically analysed orthogneiss samples grouped by area and rock complex on map with selected lithological units and outline of magnetic highs (compare with Figs. 1 and 4). Pie charts illustrate percentages of rock types defined by their chemistry within each area or complex (Table 2).

from aeromagnetic highs therefore indicate that the rock bodies causing the magnetic anomaly are buried underneath rocks with a low amount of magnetic minerals.

Fig. 6A shows the magnetic fraction of stream sediment samples, i.e. the proportion by weight of magnetic minerals in the samples. A considerable variation over the region is noticed. High contents are seen in the magnetically high areas, Isortoq, northern part of Qullugiannuit and northern Tuno areas, whereas low contents occur within magnetically low areas, Alangua, K-F zone as well as in samples from the Nuuk terrane assemblage. The Fiskefjord area shows variable to high magnetic fractions. Low content of magnetic minerals is recorded in samples from the Taserssuaq complex, eastern Nordlandet indicating that the exposed rocks are not the cause of the aeromagnetic highs. The Finnefeld complex shows low contents of magnetic minerals. A few samples with high magnetic fraction are seen among the low magnetic fraction samples within the Four lakes area.

#### 4.2.2. Nickel content

The Ni concentrations over the region (Fig. 6B) ranges from below the detection limit of 10 ppm to 1500 ppm, the highest concentration obtained in a sediment from a stream draining one of the ultramafic complexes in the area around inner Fiskefjord (Garde, 1989; Szilas et al., 2018). Stream sediment samples with elevated to high Ni contents are associated with mapped occurrences of mafic and ultramafic rocks, compare Fig. 1. The Ni distribution therefore reflects the abundance of these rocks in less known areas. Variable to high Ni in samples from Isortoq, Qullugiannuit areas and Alangua complex, and also in northern Tuno terrane, indicates that they resemble the Fiskefjord complex with regard to abundance of mafic rocks. A low-magnetic band in the eastern Isortoq area, north and north-east of Finnefeld complex (Fig. 2A, 6A), have low content of magnetic minerals as well as low Ni consistent with derivation from felsic gneiss. The low Ni in the Finnefeld and Taserssuaq complexes and in an area northwest of northern Taserssuaq agrees with the field observations that these complexes have

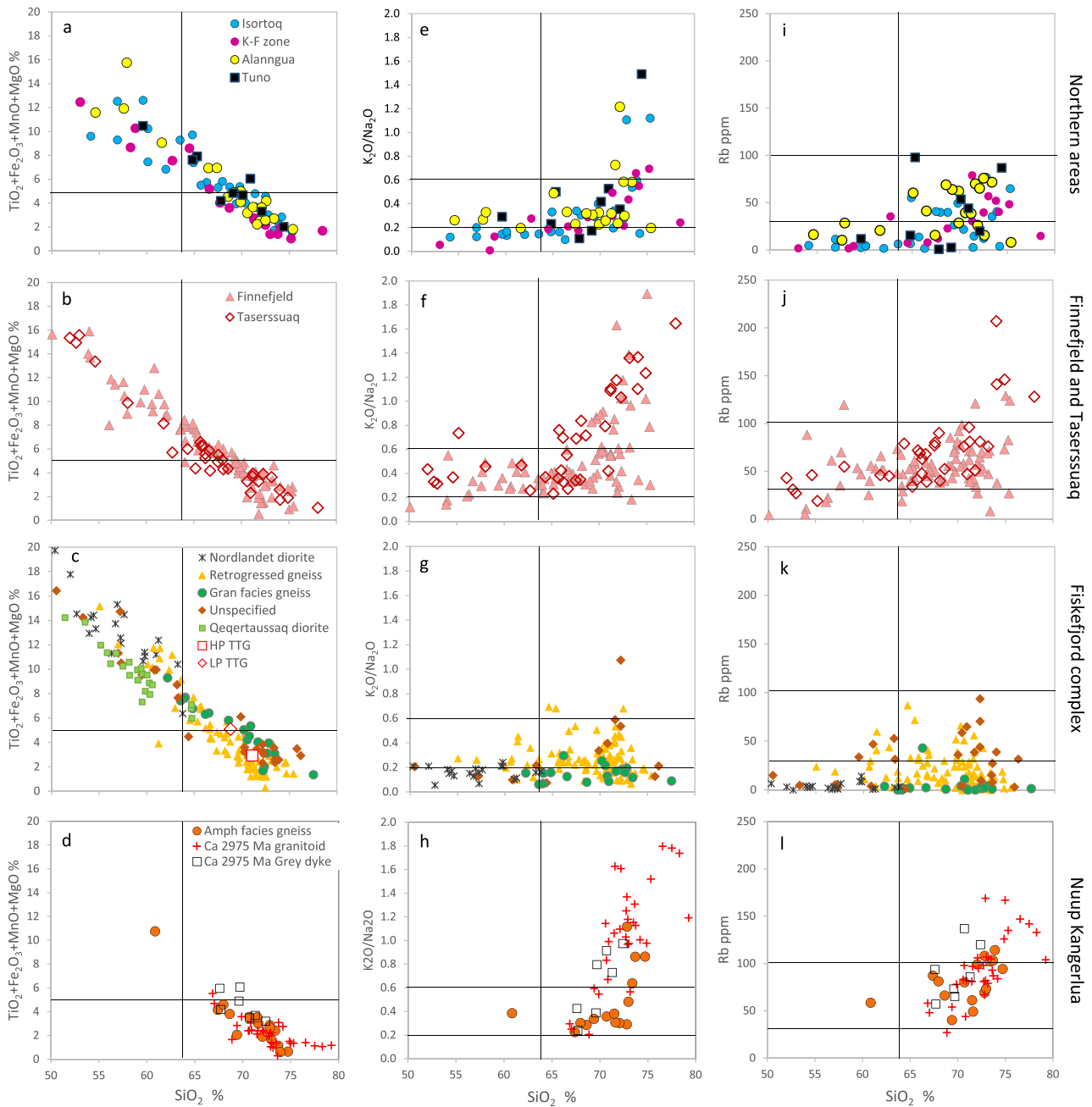


**Fig. 8.** Variation diagrams for whole rock analytical data grouped by area or complex. Reference lines correspond to limits for TTG s.s composition (Moyen and Martin, 2012):  $\text{SiO}_2 > 64\%$ , “mafic index” (sum of  $\text{TiO}_2$ ,  $\text{Fe}_2\text{O}_3$ ,  $\text{MnO}$  and  $\text{MgO}$ )  $< 5\%$  and  $\text{K}_2\text{O}/\text{Na}_2\text{O} < 0.6$ . An extra reference line in the central panel at  $\text{K}_2\text{O}/\text{Na}_2\text{O} = 0.2$  is added to ease the distinction between granulite facies mafic gneiss in Isortoq and Fiskefjord areas and orthogneiss of the Finnefjeld-Taserssuaq complexes, as are reference lines  $\text{Rb} = 30$  and  $100$  ppm, respectively, in diagrams of the right column.

very few enclaves of mafic metavolcanic rocks. Low Ni in the south-eastern part of the Tuno terrane is presently unaccounted for. The metanorite bodies of the Norite Belt (Fig. 1A) are enriched in Ni, but as the bodies are small, their contribution to the stream sediment Ni distribution is not clearly discernible at the density of sampling and scale of the figure.

#### 4.2.3. Rubidium content

Rubidium is an incompatible element that becomes enriched in magmatically differentiated melts and preferentially enters felsic melts during anatexis. Thus, Rb extracted from the deep crust during high-grade metamorphism and partial melting concentrates in the upper crust during felsic magma accumulation (Rudnick and Gao, 2014). The

variation in the Rb content of the rocks is transferred to stream sediments, which can then provide information on rock types and metamorphic grade.

Samples across the study area show a large variation in Rb, from close to the detection limit to a maximum of 300 ppm (Fig. 6C). High Rb is spatially correlated with low-magnetic areas in the Alangua complex, an area within the Tuno terrane, the Four Lakes and Nuup Kangerlua areas and in most of the Nuuk terrane assemblage. Low Rb occurs in the southwestern part of the Fiskefjord complex, the western Isortoq area, northwesternmost Tuno terrane and Tuno keel. The Rb concentration varies between moderate and high in the northern areas and within the Finnefjeld and Taserssuaq complexes. Samples with elevated concentrations occur in the south-eastern part of Nordlandet, where

anatexis is observed (McGregor et al., 1984).

#### 4.3. Whole rock geochemistry

Whole rock geochemical data are used here to provide information on the character of the crust-forming felsic to intermediate plutonic rocks, the orthogneiss, across the study region. Data from 428 samples of felsic and intermediate plutonic rocks (279 from the Fiskefjord map sheet, Garde 1997, and 155 provided by MMR) are used in this study. Data from samples of small gabbroic and ultramafic units as well as pegmatite, small granites and neosome are omitted, except cognate mafic plutonic inclusions in the Finnefeld and Taserssuaq complexes, which are important to understand the petrogenesis of these plutons. Analytical data are provided in Supplementary Table S1.

Fig. 7 shows the location and coverage of rock samples included in the diagrams of Fig. 8. In both figures, samples are grouped according to the areas outlined by geological mapping combined with aeromagnetic data (Fig. 3). The distribution of rock samples is irregular, and samples are missing from Qullugiannuit, Four lakes, parts of Taserssuaq and southern Nordlandet areas. Some symbols hide samples collected at the same site, but these appear in the variation diagrams of Fig. 8. Sampling of the Taserssuaq complex is biased with 7 samples from the northern part and 27 from the southernmost part (Fiskefjord map sheet) of which six are mafic enclaves. The Finnefeld complex is represented by 50 samples from the main part and 34 samples located in the southern extension, within the Fiskefjord map sheet. Samples with more mafic composition than TTG ( $\text{SiO}_2 < 64\%$ , Moyen, 2011) are marked with a black cross in the symbol. In the Fiskefjord complex, the samples are from Garde (1997), except those labelled “Unspecified” which are MMR samples and for which the metamorphic grade was not registered. The Fiskefjord diagrams for  $\text{K}_2\text{O}/\text{Na}_2\text{O}$  and for Rb do not include the dioritic map units, Nordlandet and Qeqertausaag diorites.

Variation diagrams for  $\text{SiO}_2$  versus the sum of mafic components, potassium relative to sodium and rubidium, respectively, illustrate main features of the orthogneiss samples within each area. The diagram for Nuup Kangerlua also contains samples of younger granitoids, which all occur along the western edge of the Taserssuaq complex (Fig. 7). The diagrams show that all areas have a large spread in orthogneiss compositions from almost gabbroic to granitic. The reference lines illustrate that many samples do not classify as TTG *sensu stricto* (s.s.) for which the “mafic index” (an unofficial term used here for the sum of  $\text{TiO}_2$ ,  $\text{Fe}_2\text{O}_3$ , MnO and MgO) should be  $< 5\%$  and  $\text{K}_2\text{O}/\text{Na}_2\text{O} > 0.6$ , according to Moyen and Martin (2012). A large proportion is too mafic (dioritic) another smaller part is too potassic or granitic in composition as illustrated by pie charts in Fig. 7 based on Fig. 8 and data in Table 2. The geological map of Nordlandet shows large areas of metadiorite and this rock type is also common although in smaller bodies in the central part of the Fiskefjord complex (Garde, 1997).

A plot of  $\text{SiO}_2$  against  $\text{K}_2\text{O}/\text{Na}_2\text{O}$  (Fig. 8, central column) reveals some differences between the areas. Fiskefjord samples and the non-retrogressed granulite-facies rocks, in particular are sodic ( $\text{K}_2\text{O}/\text{Na}_2\text{O} < 0.2$ ). In other areas, most samples with  $\text{SiO}_2 > 64\%$  have  $\text{K}_2\text{O}/\text{Na}_2\text{O}$  between 0.2 and 0.6, whereas the Finnefeld and Taserssuaq complexes exhibit higher  $\text{K}_2\text{O}/\text{Na}_2\text{O}$  for both mafic and siliceous samples and a higher proportion of samples above 0.6. The Nuup Kangerlua diagram (Fig. 8h) shows that the amphibolite-facies orthogneiss of the Fiskefjord complex is sodic to potassic and the late granitoids are, expectedly, potassic to granitic.

The orthogneiss samples from the northern areas show mutually similar variation in Fig. 8a. In Fig. 8e, the Alannua complex has  $\text{K}_2\text{O}/\text{Na}_2\text{O}$  between 0.2 and 0.4, Isortoq samples around 0.2, whereas K-F zone samples gradually increase in  $\text{K}_2\text{O}/\text{Na}_2\text{O}$  with increasing  $\text{SiO}_2$ . Tuno samples are variable with half of the samples below 30 ppm Rb and none exceeding 100 ppm (Fig. 8i). Four samples from the Tuno terrane

with Rb  $> 40$  ppm are collected within an area outlined in Fig. 8, which also shows high stream sediment Rb (Fig. 6C), but the reason for the elevated Rb is presently not known.

The Finnefeld and Taserssuaq complexes are chemically similar, and distinct from other areas: mafic samples are less scattered along the general trend, there is a higher abundance of samples with mafic index above 5% in the interval 65–70%  $\text{SiO}_2$ , fewer samples with  $\text{K}_2\text{O}/\text{Na}_2\text{O} < 0.2$ , and for samples with  $\text{SiO}_2 > 65\%$ ,  $\text{K}_2\text{O}/\text{Na}_2\text{O}$  increases with increasing  $\text{SiO}_2$  to reach granitic compositions ( $\text{K}_2\text{O}/\text{Na}_2\text{O} > 1$ ). The Rb contents are consistently above 30 ppm Rb and generally vary between 50 and 100 ppm Rb, similar to the samples of amphibolite-facies orthogneiss of the Nuup Kangerlua area (Fig. 8l). Even the most mafic Finnefeld and Taserssuaq samples have Rb  $> 30$  ppm, in contrast to gneiss in the northern areas (Fig. 8i) and in the Fiskefjord complex (Fig. 8k), where many samples have  $< 30$  ppm.

#### 4.4. Geochronology

Published zircon U-Pb isotope data are available for 107 samples within the Maniitsoq region. Additionally, U-Pb data for fifteen new samples are presented in this work to fill in the coverage of dated samples within the study area and to address some unsolved issues including: 1). The position of the boundary between the Alannua complex and Tuno terrane (237); 2). Neoarchaean reworking within the Alannua (orthogneiss 301, 302, 316, 541, 1006, paragneiss 464, 543) and Finnefeld complex (orthogneiss 212, 213, 218); 3). Age relationships within the Kangia-Fossilik zone (orthogneiss 582) and Taserssuaq magnetic high (grey dyke 896), and finally ages of orthogneiss components in the Fiskefjord complex (567, 311).

##### 4.4.1. New dated samples

Individual sample concordia plots, measured U-Pb isotope data and cathodoluminescence (CL) images of all zircon grains for the new samples reported in this work are provided in Supplementary files S2–S4, respectively. Fig. 9 provides examples of CL images of analysed grains. Table 1 and Fig. 10 provide sample locations. All ages are reported with  $\pm 2\sigma$  uncertainties unless specifically stated otherwise.

**4.4.1.1. Tuno terrane.** Sample 237, granulite-facies felsic orthogneiss. The zircon crystals are euhedral to subhedral, generally have slightly rounded terminations and range in length from 100  $\mu\text{m}$  to 200  $\mu\text{m}$ . Fourteen analyses of oscillatory zoned zircon yield a weighted mean  $^{207}\text{Pb}/^{206}\text{Pb}$  age of  $2819 \pm 4$  Ma (MSWD = 2), interpreted as the magmatic age of the rock. Two analyses of oscillatory zoned cores yield  $^{207}\text{Pb}/^{206}\text{Pb}$  ages of 2957 and 2975 Ma, interpreted as the age of xenocrystic zircon. Two analyses sited on homogeneous rims, have low apparent alpha doses, low Th and U and yield a weighted mean  $^{207}\text{Pb}/^{206}\text{Pb}$  age of  $2733 \pm 11$  Ma (MSWD 0.54), interpreted as a time of granulite-facies metamorphism.

**4.4.1.2. Alannua complex.** Sample 316, tonalitic component of poly-phase gneiss (diorite and amphibolitic enclaves) with foliation-parallel leucosome. The zircon crystals are subhedral to euhedral. In CL images, oscillatory zoning in cores is common and all grains have a low CL response (high U) overgrowth up to 50  $\mu\text{m}$  thick. Fourteen analyses of oscillatory zoned cores yield  $^{207}\text{Pb}/^{206}\text{Pb}$  ages in the intervals 3285–3216 Ma and 3097–3054 Ma are interpreted as the age of protolith components, which agrees with the polyphase nature of the rock. One grain yields a  $^{207}\text{Pb}/^{206}\text{Pb}$  age of  $2879 \pm 8$  Ma and may date a minor late magmatic component. Three analyses of homogenous rims yield a weighted mean  $^{207}\text{Pb}/^{206}\text{Pb}$  age of  $2685 \pm 14$  Ma (MSWD = 1.7), interpreted as the age of high-grade metamorphism. Sample 541, trondhjemitic orthogneiss with mafic enclaves crosscut by leucosome veins. The zircon crystals are anhedral to euhedral, rounded to

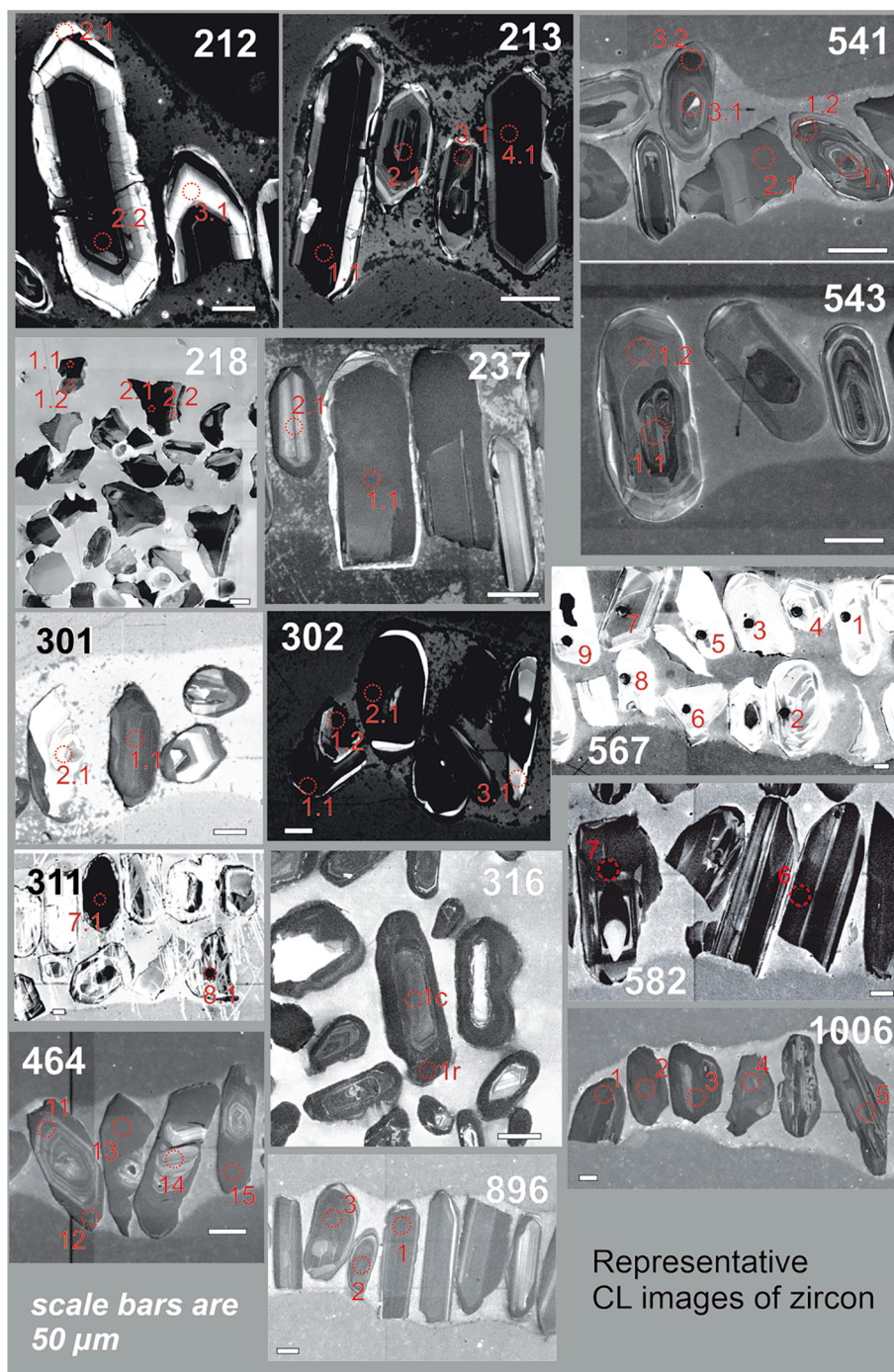


Fig. 9. Cathodoluminescence images with sample ID for selected zircon grains used for U-Pb age dating described in Section 4.4.

prismatic, with highly variable length to width ratios. In CL images, idiomorphic zoning is common, and most grains have a low CL response (high U) overgrowth up to 30  $\mu\text{m}$  thick. Internal textures in some grains imply many phases of dissolution and new growth. The best estimate for the original protolith age is  $3068 \pm 4$  Ma (MSWD = 1.1) based on the oldest statistically coherent group of five analyses of oscillatory zoned grains within a group of zircon analyses classified as mixed. The youngest grouping of three analyses yields a weighted mean  $^{207}\text{Pb}/^{206}\text{Pb}$  age of  $2554 \pm 8$  Ma (MSWD = 0.42); these analyses were sited on either sector zoned cores of distinctly large grains or within a homogeneous

rim. This age is interpreted as the crystallization age of zircon within cross cutting plagioclase bearing leucosomes that intrude this gneiss. Sample 1006, ca. 10 m wide metadiorite body surrounded by strongly banded and strained felsic orthogneiss. The zircon crystals are anhedral and have low to moderate length to width ratios of 1:1 to 4:1. Two analyses were taken on grain cores, exhibiting convolute or oscillatory zoning and partially resorbed edges. These grains have moderate U concentrations (88–235 ppm), moderate Th/U ratios (0.53–1.24) and yield  $^{207}\text{Pb}/^{206}\text{Pb}$  dates from  $2791 \pm 13$  Ma to  $2771 \pm 18$  Ma and are interpreted to reflect xenocrystic components. If undisturbed, these core

**Table 1**  
Published and new interpreted zircon  $^{207}\text{Pb}/^{206}\text{Pb}$  ages with sample location and references. Number of determined ages are noted in each of eight age intervals. Supracrustal rocks comprise metasedimentary and metavolcanic (volc) rocks. Description of new data in section 4.4, additional documentation for new data in Supplementary files S2–S4.

SampleID	Area	Interpreted magmatic age Ma	3800–3600	3300–3100	3100–3015	3015–2990	2990–2900	2900–2800	2800–2700	2700–2500	Latitude	Longitude	Reference
<b>Orthogneiss</b>													
237	Tuno	2819, 2733 M					2X	14		2 M	65.4124	–52.9002	This paper
250	Tuno keel	2998			1	5	4	1 M	1 M		65.3572	–52.7112	Kirkland et al.2016
G94/1	Tuno keel	2982, 2816 M					13	16 M			65.4250	–52.5378	Garde et al.2000
235	Alanngua	2992				8	8				65.2275	–52.4884	Gardiner et al.2019
301	Alanngua	3010, 2719 M		1X	6	9			2 M		65.2335	–52.3037	This paper
302	Alanngua	none			1	1	3		4 M	1 M	65.2335	–52.3037	This paper
306	Alanngua	3019			4	4	1				65.2902	–52.3096	Gardiner et al.2019
316	Alanngua	not given		8	5			1		3 M	65.3907	–52.3949	This paper
541	Alanngua	3068			5				6 M	4 M	65.1024	–52.4299	This paper
747	Alanngua	2990				8	7				65.3562	–52.4337	Kirkland et al.2016
1006	Alanngua	not given							2X,2M		65.6722	–51.8538	This paper
525326	Alanngua	2775–				4	4		23 M		65.2566	–52.2601	Scherstén and Garde, 2013
VM 97/17	QarliitTas	not given	8				1		5 M		65.7792	–50.7207	Nutman et al. 2004
VM 97/18	QarliitTas	not given	15	2					8 M		65.7875	–50.7115	Nutman et al. 2004
524,233	Qullugiaq high	2999*			1	7	1				65.6891	–51.2098	Scherstén and Garde, 2013
159	Isortoq high	3019			6	6					65.4726	–51.8290	Gardiner et al.2019
325	Isortoq high	3002			2	7	5				65.4830	–51.9822	Gardiner et al.2019
524226	Isortoq high	3035			5	3	2				65.5167	–51.4518	Scherstén and Garde, 2013
G94/3	Isortoq high	3016, 2941 M			8	6	22 M	1	2		65.3985	–52.2435	Garde et al.2000
582	K-F zone	3014			6	9					65.4349	–51.4549	This paper
871	K-F zone	3008		1X	9X	3					65.3528	–51.4414	Olierook et al. 2020
873	K-F zone	3011			13X,4	12	1				65.3528	–51.4414	Olierook et al. 2020
1415	K-F zone	3013			18X	5					65.3528	–51.4415	Olierook et al. 2020
173	Finnefeld	3007			1	8					65.2938	–51.5956	Gardiner et al.2019
212	Finnefeld	2986				6	15			2 M	65.2951	–52.0348	This paper
213	Finnefeld	2987				3	6				65.2951	–52.0347	This paper
218	Finnefeld	not given							16		65.1926	–52.2227	This paper
307	Finnefeld	3011			3	8	1				65.3259	–52.3047	Gardiner et al.2019
407	Finnefeld	2993				12	5				65.3463	–52.1392	Gardiner et al.2019
530	Finnefeld	2998			2	14	5				65.1772	–51.9856	Gardiner et al.2019
534	Finnefeld	2998				11	3				65.1860	–51.9866	Gardiner et al.2019
575	Finnefeld	3013			2	7					65.3296	–51.7844	Gardiner et al.2019
887	Finnefeld	2992				15	5				65.1477	–52.0122	Kirkland et al., 2020
339641	Finnefeld	2975				2	15				65.0451	–52.2148	Garde et al.2000
524282	Finnefeld	3003*			2	6	1	1			65.2640	–51.6268	Scherstén and Garde, 2013
158	Finne S high	3008			2	6					65.1761	–51.5631	Gardiner et al.2019
566	Finne S high	3018			7	4	3				65.0812	–51.9220	Gardiner et al.2019
1256	Taserssuaq high	3002			2	13	4				65.3896	–51.1826	Kirkland et al., 2020
477307	Taserssuaq high	3006			1	7	1				64.7075	–50.7845	Hollis, 2005
524261	Taserssuaq	2995				6	3				65.3681	–50.9687	Scherstén and Garde, 2013
524204	Taserssuaq high	3000*				8	2				65.3350	–51.1950	Scherstén and Garde, 2013
524216	Taserssuaq high	3000*			2	8	5				65.3397	–51.2155	Scherstén and Garde, 2013
D73	Taserssuaq	2991**				5					65.1166	–50.2878	Hanmer et al. 2002

(continued on next page)

Table 1 (continued)

SampleID	Area	Interpreted magmatic age Ma	3800–3600	3300–3100	3100–3015	3015–2990	2990–2900	2900–2800	2800–2700	2700–2500	Latitude	Longitude	Reference
220	Fiskefjord	3231		28							64.9704	−52.2985	Gardiner et al.2019
186456	Fiskefjord	2978				3	37	2	1		64.9896	−51.5523	Szilas et al. 2018
289246	Fiskefjord	3050, 3026			15	4					64.7244	−51.2894	Garde et al.2000
339199	Fiskefjord	3035, 2981 M			7	4	9 M				64.8237	−52.0256	Garde et al.2000
339223	Fiskefjord	3044			11	1					64.8838	−51.6095	Garde et al.2000
477678	Fiskefjord	3058			21	7					64.8422	−51.1336	Garde et al., 2012c
283672	Nordlandet	3221		10							64.5800	−51.6558	Garde 1997
278886	Iganannguit	3008X, 2971				2X	5				65.1061	−51.0647	Garde et al.2000
289177	Qussuk granite	3001X, 2975			3X	5X	9				64.8483	−51.1711	Garde et al.2000
289278	Nuup	3021			4	4	3				64.6637	−51.1858	Naeraa et al., 2012
	Kangerlua												
283347	Nuup	3038			17	2	5				64.6680	−51.1509	Naeraa et al., 2012
	Kangerlua												
477321	Nuup	3040			14	1	1				64.6082	−51.0449	Hollis, 2005
	Kangerlua												
479606	Nuup	3064			37						64.2829	−51.4562	Hollis, 2005
	Kangerlua												
479703	Nuup	2840						29			64.2698	−51.4437	Hollis, 2005
	Kangerlua												
481201	Nuup	3072	1		26	1	1				64.5510	−50.9971	Hollis, 2005
	Kangerlua												
481227	Nuup	3046			20	1	3				64.4567	−51.0923	Hollis, 2005
	Kangerlua												
481311	Nuup	3048			19	3	3	1			64.4547	−51.0908	Hollis, 2005
	Kangerlua												
479060	Nuup	3048			10		2		1	3	64.3874	−51.2544	Hollis, 2005
	Kangerlua												
479813	Nuup	3050			7	12	6				64.3800	−51.3544	Hollis, 2005
	Kangerlua												
499339	Nuup	2984				11	23	7			64.1921	−51.7036	Naeraa et al., 2012
	Kangerlua												
<b>Late intrusive bodies</b>													
740	Tuno	3009 M			2 M	9 M					65.4713	−53.0713	Yakymchuk et al. 2020
310	Alanngua	2538								5	65.2989	−52.3285	Kirkland et al., 2020
318	Alanngua	2729							13		65.2962	−52.4528	Gardiner et al.2019
704	Alanngua	2729							10		65.1302	−52.4216	Gardiner et al.2019
872	K-F zone	2980				7X,4	24				65.3528	−51.4414	Olierook et al. 2020
1416	K-F zone	none			4X		3X				65.3528	−51.4415	Olierook et al. 2020
1417	K-F zone	2973			2X	1X	18				65.3528	−51.4415	Olierook et al. 2020
524254	K-F zone	2969					10				65.3526	−51.4392	Scherstén and Garde, 2013
215	Finnefjeld	2558			2		3	1	1	24	65.1926	−52.2227	Gardiner et al.2019
216	Finnefjeld	3059X, 2994X			11	4					65.1926	−52.2227	Kirkland et al., 2018
567	Finne S high	2998			2	6	7				65.0812	−51.9224	This paper
524217	Taserssuaq	3003*				10	2				65.3391	−51.2142	Scherstén and Garde, 2013
896	Taserssuaq high	2970		1X		9X	4,2X				65.3385	−51.2187	This paper
202	Fiskefjord	3000			2	11	4				65.0096	−51.6756	Yakymchuk et al. 2020
221	Fiskefjord	2977			1	1	11 M				64.9704	−52.2985	Gardiner et al.2019
222	Fiskefjord	3240		16X	1						64.9704	−52.2985	Gardiner et al.2019
224	Fiskefjord	2986			1	3	9				65.0380	−52.1940	Gardiner et al.2019
311	Fiskefjord	3006				7					64.9547	−52.1324	This paper
507	Fiskefjord	3008			2	6					64.9636	−52.1421	Gardiner et al.2019
186451	Fiskefjord	2969				6	38	1			64.9878	−51.5555	Szilas et al. 2018

(continued on next page)

Table 1 (continued)

SampleID	Area	Interpreted magmatic age Ma	3800–3600	3300–3100	3100–3015	3015–2990	2990–2900	2900–2800	2800–2700	2700–2500	Latitude	Longitude	Reference
186453	Fiskefjord	2940				2	69	15			64.9875	–51.5514	Szilas et al. 2018
SampleA	Fiskefjord	2990				6	4				64.9280	–51.4272	Nilsson et al. 2010
484657	Nordlandet	3238		10	3		1				64.5573	–51.9113	Naeraa et al., 2012
477318	Nuup Kangerlua	2990				6	5				64.6581	–50.9696	Garde 2007
477320	Nuup Kangerlua	3005X, 2992				9	1				64.6550	–50.9774	Garde 2007
477352	Nuup Kangerlua	2984				4	14	2	1		64.6743	–51.0423	Garde 2007
479049	Nuup Kangerlua	3055			26	1	2	1			64.3594	–51.3073	Hollis, 2005
479301	Nuup Kangerlua	2840						22			64.2539	–51.4677	Hollis, 2005
479665	Nuup Kangerlua	3053			13						64.4214	–51.2394	Hollis, 2005
<b>Supracrustal rocks</b>													
483	Tuno								17 M		65.6767	–52.7807	Gardiner et al. 2019
VM97/12	Tuno			4	9	16	17	4			65.5995	–52.8427	Nutman et al. 2004
319	Tuno keel		1	48	5	19	5 M	3 M			65.4462	–52.5854	Kirkland et al. 2018
303	Alanngua			3	2	7	1 M	15 M	2 M		65.2570	–52.2828	Kirkland et al. 2018
309	Alanngua			4			1 M				65.2433	–52.3703	Yakymchuk et al. 2020
315	Alanngua		1	3	16	22	2			4 M	64.9741	–52.4151	Kirkland et al. 2018
464	Alanngua		4	13	3	2	1	1 M	11 M		65.5681	–52.3900	This paper
535	Alanngua			3	3	3	1 M	2 M	3 M		64.9671	–52.4128	Gardiner et al. 2019
537	Alanngua			8	4	1		1 M			64.9741	–52.4151	Gardiner et al. 2019
543	Alanngua			4	3	3	3	19 M	1 M		65.1081	–52.4565	This paper
729	Alanngua		2	43	16	11					64.9542	–52.4075	Kirkland et al. 2018
739	Alanngua			5	2	1					65.4128	–52.5225	Gardiner et al. 2019
524906	Alanngua			2	1	3	4	6	40 M		65.4216	–52.5050	Dyck et al. 2015
524907	Alanngua			4	5	3	2	4	59 M		65.4216	–52.5050	Dyck et al. 2015
G94/2	Alanngua		6	1	1	1			12 M		65.4133	–52.5233	Garde et al. 2000
313	Fiskefjord			8	9	8	2 M	16 M			64.9547	–52.1324	Kirkland et al. 2018
477367	Nuup K (volc)	2975 M		3	2	13 M					64.6664	–51.1268	Garde2007
477385	Nuup K (volc)	2984 M		1	5	10 M	1				64.6694	–51.1226	Garde2007
477629	Nuup K (volc)	2997 M				5 M	3 M				64.7872	–51.1081	Garde et al., 2012c
477630	Nuup Kangerlua					3 M	2 M				64.7769	–51.0964	Garde et al., 2012c
477635	Nuup Kangerlua			11	9 M	1 M					64.7879	–51.0959	Garde et al., 2012c
479052	Nuup K (volc)	2834						10			64.3620	–51.2987	Hollis, 2005
479326	Nuup Kangerlua						2	26	1	1	64.2708	–51.4295	Hollis, 2005
479681	Nuup K (volc)			23							64.4211	–51.2565	Hollis, 2005
479745	Nuup K (volc)						1	21	2		64.4400	–51.2953	Hollis, 2005
479814	Nuup Kangerlua		1	1	11 M	13 M	1				64.3846	–51.3357	Hollis, 2005
479827	Nuup K (volc)	3071		20	1						64.4398	–51.3089	Hollis, 2005
488103	Nuup K (volc)	2988 M				3	12 M		1		64.4400	–51.2953	Garde et al., 2012c

–age regarded equivocal by Scherstén and Garde 2013

\*interpreted as age of hydrothermal alteration

\*\* TIMS data

M:age of metamorphism

X: age of xenocrysts

ages represent a maximum age for the diorite. Two analyses were conducted on zircon with homogenous CL response. These analyses indicate moderate U concentrations (192–205 ppm), moderate Th/U ratios (0.48–0.49), and yield  $^{207}\text{Pb}/^{206}\text{Pb}$  dates of  $2784 \pm 14$  Ma (whole-grain) and  $2753 \pm 15$  Ma (grain mantle). These analyses may represent metamorphic zircon growth or partial resetting of the U-Pb system and provide a maximum age for one episode of metamorphism. Sample **464**, paragneiss with corundum at contact to ultramafic body. The zircon crystals are sub-rounded to sub-angular and have low to moderate length to width ratios of 1:1 to 4:1. Twenty-three analyses conducted on detrital grains indicate  $^{207}\text{Pb}/^{206}\text{Pb}$  dates between 3131 and 2861 Ma, the youngest of which ( $2861 \pm 15$  Ma) represents a maximum depositional age for the sample. The detrital grains define significant age components at c. 3033 and 3072 Ma, and several minor components within the range 2953–3108 Ma. These ages are interpreted as the ages of zircon-crystallizing rocks in the detrital source region(s), or as the ages of detrital components within sediments that have been reworked into this rock. Sample **543**, garnet-sillimanite pelite. The zircon crystals are subhedral to euhedral, with rounded terminations. In CL images, idiomorphic zoning is common. Ten analyses on oscillatory-zoned grains yield  $^{207}\text{Pb}/^{206}\text{Pb}$  ages of 3010–2880 Ma, interpreted as the age of detrital components. Taking a conservative approach and accepting only the most concordant of these analyses as being unaffected by radiogenic-Pb mobility implies a maximum depositional age of  $2961 \pm 8$  Ma. Eighteen analyses principally located on overgrowths that mantle oscillatory zoned cores spread on concordia with  $^{207}\text{Pb}/^{206}\text{Pb}$  ages of 2778 Ma to 2702 Ma. These analyses may reflect new metamorphic zircon growth and partial to near complete radiogenic-Pb loss in precursor domains. One rim analysis yields a  $^{207}\text{Pb}/^{206}\text{Pb}$  age of  $2598 \pm 18$  Ma and may reflect a later metamorphic zircon growth event

#### 4.4.1.3. Boundary zone between Finnefjeld and Alanngua complexes..

Sample **301**, intermediate orthogneiss in folded package. The zircon crystals are euhedral to subhedral, generally have slightly rounded terminations and range in length from 100  $\mu\text{m}$  to 150  $\mu\text{m}$ . Under CL the grains reveal oscillatory zoning. Some grains have CL dark homogeneous rims. Fifteen analyses of oscillatory zoned zircon yield a weighted mean  $^{207}\text{Pb}/^{206}\text{Pb}$  age of  $3010 \pm 7$  Ma (MSWD 2.5), interpreted as the magmatic age of the rock. One analysis of an oscillatory zoned core yields a  $^{207}\text{Pb}/^{206}\text{Pb}$  age of  $3202 \pm 6$  Ma, interpreted as the age of xenocrystic zircon. Two analyses sited on homogeneous rims yield a weighted mean  $^{207}\text{Pb}/^{206}\text{Pb}$  age of  $2719 \pm 6$  Ma (MSWD 1.01), interpreted as a time of high-P granulite-facies metamorphism. Sample **302**, Same place as 301, Felsic orthogneiss, isoclinally folded. The zircon crystals are subhedral, with moderate to high length to width ratios and rounded terminations. In CL images, oscillatory zonation in cores is common, all grains have multiple low CL response, homogeneous, overgrowths. Five core analyses yield  $^{207}\text{Pb}/^{206}\text{Pb}$  ages of 3039–2910 Ma, interpreted as the age of xenocrystic components. Six rim analyses sited on different generations of homogeneous rim (on the basis of cross cutting relationships) yield  $^{207}\text{Pb}/^{206}\text{Pb}$  ages of 2762–2686 Ma, which are interpreted as the age of a prolonged metamorphic zircon growth period.

4.4.1.4. *Finnefjeld complex.* Sample **212**, adjacent to Kangia shear zone, coarse-grained hornblende orthogneiss with relict phenocrystic fabric and strong, steep N-striking foliation. The zircon crystals are subhedral to euhedral and typically elongate. Oscillatory-zoned cores are common, and many grains are overgrown by very thin homogeneous high CL response rims. Twenty-one analyses of oscillatory-zoned zircon yield a weighted mean  $^{207}\text{Pb}/^{206}\text{Pb}$  age of  $2986 \pm 5$  Ma (MSWD = 2.1), interpreted as the age of magmatic crystallization of the rock. One analysis with a  $^{207}\text{Pb}/^{206}\text{Pb}$  age of  $2882 \pm 32$  Ma, dominantly sited on high CL response zircon, is nonetheless interpreted to be an inadvertent core – rim mixture. Two analyses on high CL response rims, indicate low Th/U

ratios of < 0.05, yield a weighted mean  $^{207}\text{Pb}/^{206}\text{Pb}$  age of  $2650 \pm 38$  Ma (MSWD = 0.36), interpreted as the age of metamorphic zircon growth. Sample **213**, adjacent to Kangia shear zone, same locality as sample 212, coarse-grained hornblende orthogneiss. The zircon crystals are subhedral to euhedral and typically elongate. Oscillatory zonation is common, as are resorbed domains; some grains are overgrown by very thin homogeneous high CL response rims. Eight analyses of oscillatory zoned zircon yield a weighted mean  $^{207}\text{Pb}/^{206}\text{Pb}$  age of  $2987 \pm 6$  Ma (MSWD = 1.0), interpreted as the age of magmatic crystallization of the rock. Sample **218**, close to Kangia shear zone and boundary to Alanngua complex. Highly strained medium-grained hornblende granodioritic gneiss. The zircon crystals are anhedral to subhedral and many have distinctive angular or broken faces, which is unlikely to be a processing artefact. In CL images the grains display a wide range of internal textures including broad homogenous patches, oscillatory zoning, and some grains have partially reabsorbed domains. All grains display unconformable surfaces indicative of a multistage growth history. Sixteen analyses yield a continuous distribution of  $^{207}\text{Pb}/^{206}\text{Pb}$  ages between 2775 and 2708 Ma, which may reflect prolonged zircon growth processes in the deep crust in that period or a partially effective ancient radiogenic-Pb mobility process.

4.4.1.5. *Kangia-Fossilik zone and Taserssuaq high.* Sample **582**, orthogneiss cross-cutting metanorite. The zircon crystals are euhedral with moderate to high length to width ratios of up to 6:1. In CL images the grains display faint idiomorphic zoning and generally emit low CL response (high U). All 15 analyses yield a weighted mean  $^{207}\text{Pb}/^{206}\text{Pb}$  age of  $3014 \pm 8$  Ma (MSWD = 0.41), interpreted as the age of magmatic crystallization. Sample **896**, grey dyke, fine-grained, ca. 40 cm wide. The zircon crystals are anhedral and have low to high length to width ratios of 2:1 to 5:1. Ten analyses are from grain cores with oscillatory zoning and partially resorbed to rounded edges. These grains have  $^{207}\text{Pb}/^{206}\text{Pb}$  dates from  $3017 \pm 6$  Ma to  $2959 \pm 12$  Ma interpreted as xenocrystic. Four analyses conducted on discrete grains or overgrowths with dark-oscillatory zoning in CL yielded a weighted mean  $^{207}\text{Pb}/^{206}\text{Pb}$  age of  $2970 \pm 14$  Ma (MSWD = 1.5), interpreted as recording the age of magmatic crystallization of the dyke.

4.4.1.6. *Fiskefjord complex.* Sample **311**, granitoid matrix of breccia that contains ultramafic enclaves and crosscuts foliation in package of supracrustal rocks. The zircon crystals are subhedral, rounded and range in length from 50  $\mu\text{m}$  to 150  $\mu\text{m}$ . Under CL the grains display regular oscillatory zoning. There is occasional evidence for overgrowth by a homogeneous high CL response rim. Some grains have obvious cores. Seven analyses of oscillatory zoned zircon yield a weighted mean  $^{207}\text{Pb}/^{206}\text{Pb}$  age of  $3006 \pm 11$  Ma (MSWD = 0.12), interpreted as the magmatic age of the rock. Sample **567**, felsic matrix of breccia in metanorite. The zircon crystals are euhedral. In CL images the grains display well-developed idiomorphic zoning that typically grades to CL bright margins. Fifteen analyses with 10% of concordia yield a weighted mean  $^{207}\text{Pb}/^{206}\text{Pb}$  age of  $2998 \pm 14$  Ma (MSWD = 1.3), interpreted as the age of magmatic crystallization. A sample of the prevailing orthogneiss in the surroundings (566) has an interpreted magmatic age of 3018 Ma (Table 1; Gardiner et al., 2019), which suggests that the brecciating melt is a separate intrusive event providing a minimum age of the metanorite.

#### 4.4.2. All dated samples

Results from all samples are provided in Table 1, Figs. 10 and 11. The samples are divided into three rock type groups (numbers in brackets): Orthogneiss (63), late sheets and veins (31) and supracrustal rocks (28). Late sheets and veins include granitic and other felsic sheets and dykes, pegmatites and leucosomes. The total age range recorded (3717–2519 Ma) for all samples has been divided into eight intervals, corresponding to periods of magmatism or metamorphism indicated mainly by Garde et al. (2000), Garde (2007), Kirkland et al. (2018) and Gardiner et al.

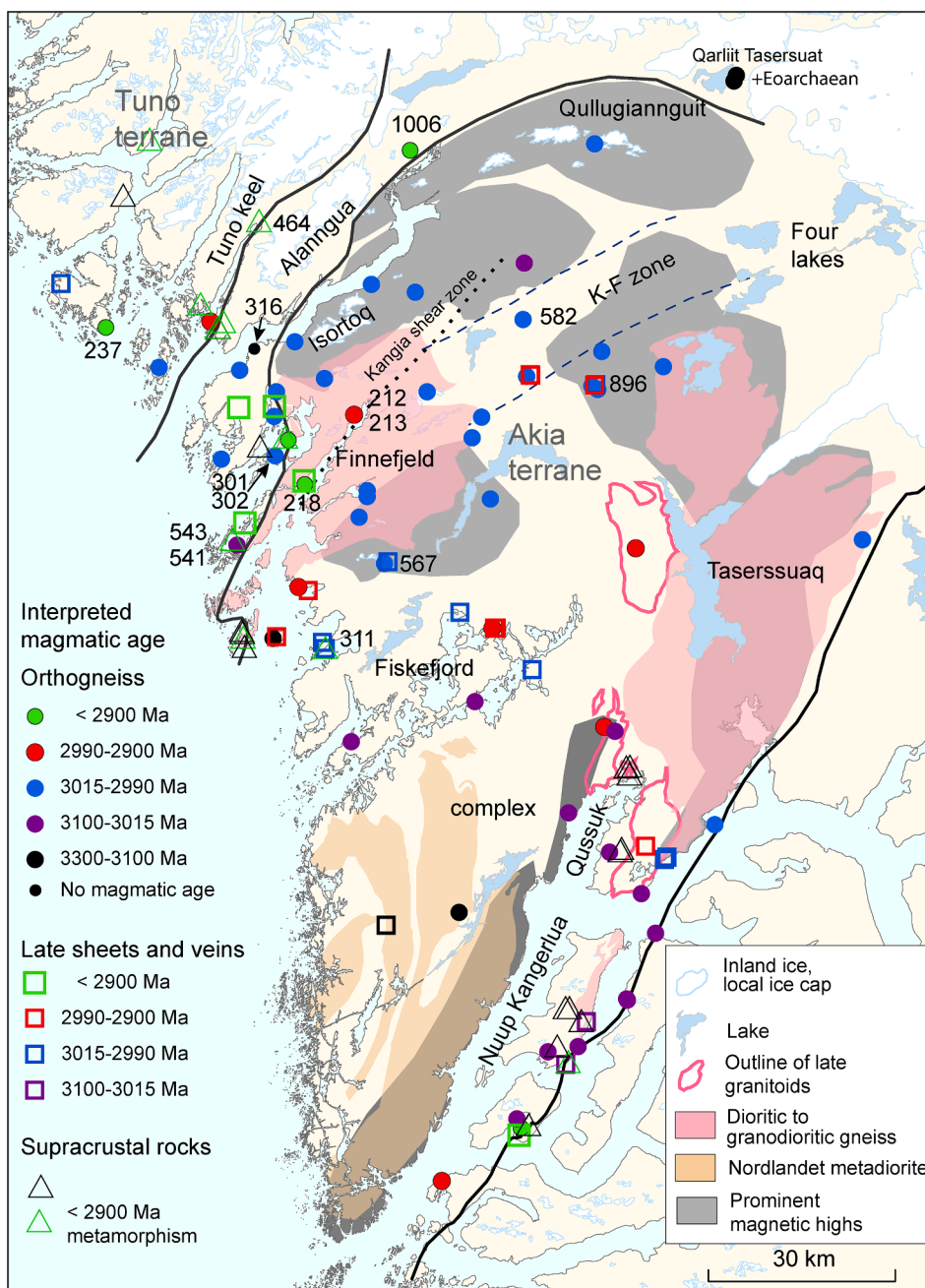


**Fig. 10.** Spatial distribution of published and new ages of zircons from samples representing three different rock types and interpreted magmatic zircon ages in time intervals corresponding to known periods of magmatism or metamorphism. Numbered samples are described in section 4.4. Background map with selected lithological units and outlined magnetic highs (compare with Figs. 1 and 4). See Table 1f or ages, geographic coordinates and literature references.

(2019). The number of measured concordant  $^{207}\text{Pb}/^{206}\text{Pb}$  ages (without those interpreted as affected by radiogenic-Pb loss) within each interval is listed in Table 1 together with the interpreted protolith age, area, geographic coordinates and where appropriate literature reference.

In Table 1, the names of lithological complexes and aeromagnetic highs are used as geographic reference names. Table 1 and Figs. 10–11 reveal significant differences between areas in terms of zircon age span. All areas have rocks with Mesoarchaeoan ages 2900–3100 Ma, but only Tuno, Alannua and Nuup Kangerlua areas plus a few samples from Finnefeld yield zircon ages < 2900 Ma. The 2900–2800 Ma magmatic ages are constrained to Tuno and Nuup Kangerlua areas, whereas the

2800–2700 Ma age group reflects the magmatic age of pegmatites and metamorphic ages of orthogneisses and supracrustal rocks in the Alannua and Tuno areas (Table 1 and Fig. 11). The geochronological data are discussed in Section 5.3.

#### 4.5. Summary of results

Table 2 summarises the results of the data sets. The chemical compositions are used to estimate the percentage of rock samples that may be termed TTG s.s. according to the definition of Moyen and Martin (2012), i.e. content of  $\text{SiO}_2 > 64\%$ ,  $(\text{TiO}_2 + \text{Fe}_2\text{O}_3\text{T} + \text{MnO} + \text{MgO}) <$

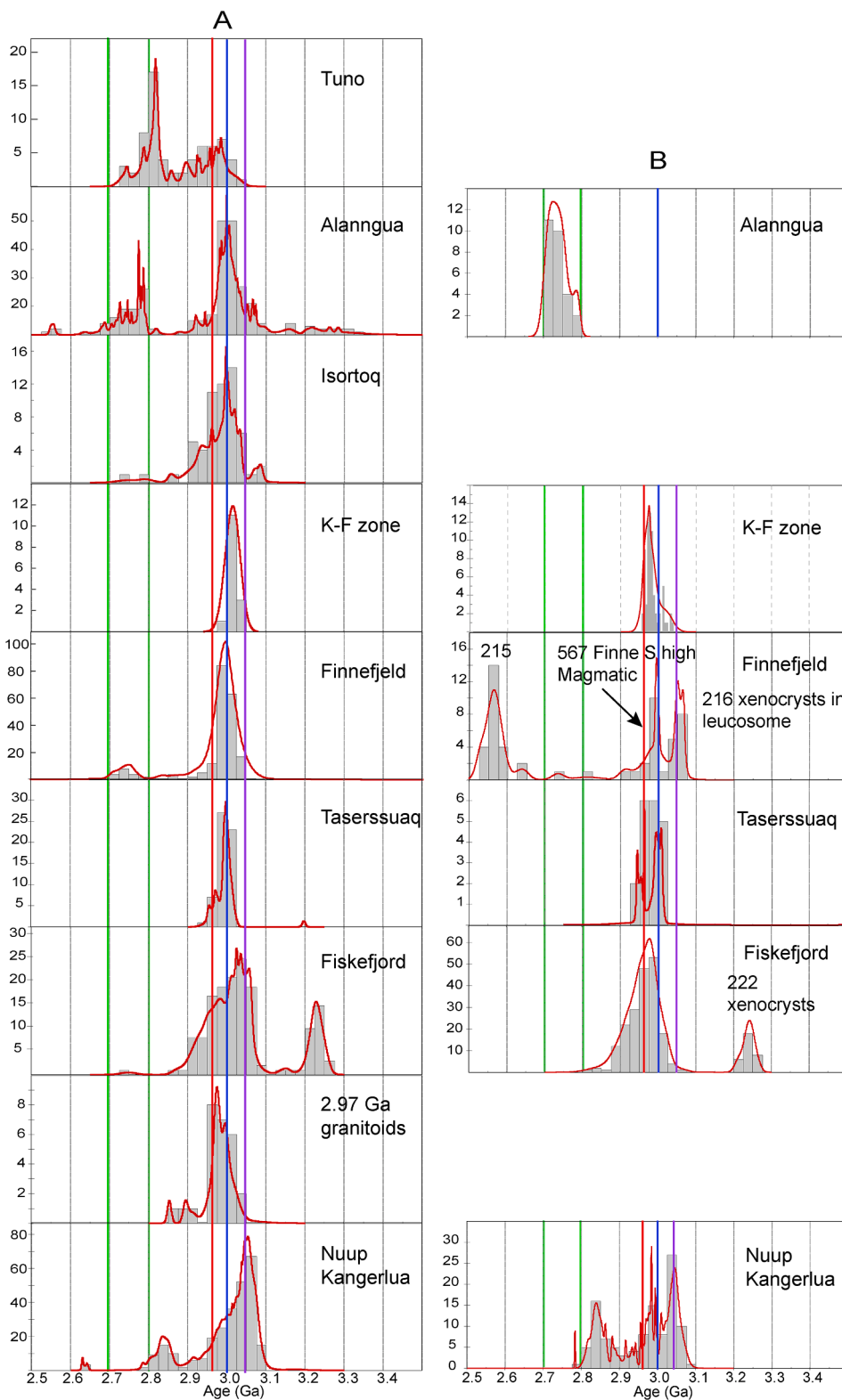


**Fig. 11.** Histogram and probability curves for zircon ages per area or complex. A: Interpreted magmatic ages of orthogneiss samples. B: interpreted magmatic ages of late sheets and felsic dykes. C: Detrital and metamorphic ages of zircons from metasedimentary rocks.

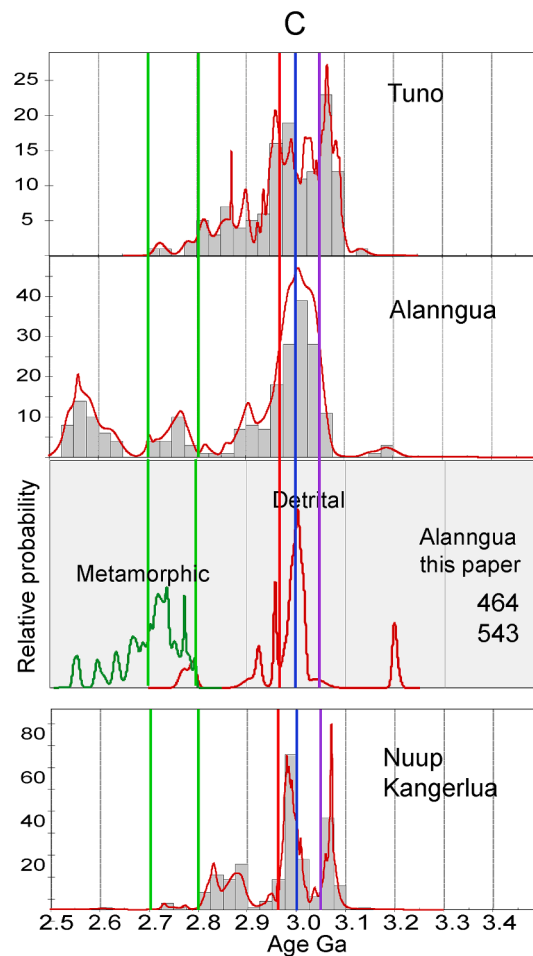


Fig. 11. (continued).

5%, and  $K_2O/Na_2O$  ratio  $< 0.6$ , (see Fig. 8). In addition, Table 2 shows percentages of samples that should *not* be classified as TTG because they are too mafic or too potassic, respectively. Only the amphibolite-facies orthogneiss within the Nuup Kangerlua-Qussuk area (Garde, 1997) can be described as largely TTG, and few samples from Finnefeld and Taserssuaq complexes are TTG s.s.

Collectively, the results indicate that the boundary between the Tuno and Akia terrane is a tectonically complicated zone comprising two shear zone-bounded segments: the Tuno keel and the Alanngua complex. Furthermore they indicate that the Akia terrane is more diverse in lithology, structure and chronology than previously recognised. Table 2 illustrates that each complex or area within the Akia terrane, has a distinct combination of large-scale structure (outlined by geological maps and aeromagnetic data), stream sediment and rock geochemistry, and timing of rock-forming events.

The Qullugiannuit and Isortoq areas are similar in structure, magnetic response and stream sediment response. The aeromagnetic anomaly associated with Qullugiannuit appears more deep-seated than that associated with the Isortoq area (Fig. 3), and the lack of rock data and field observations from Qullugiannuit makes it premature to correlate the two areas. The Finnefeld and Taserssuaq complexes are very similar in chemistry and age but are differently deformed. The two complexes are distinct from the Fiskefjord complex in all parameters. The Four lakes and Nuup Kangerlua area are similar in lithology, aeromagnetic and stream sediment geochemical data, but there are no ages

or rock samples available for the Four lakes area to permit a correlation. Neoarchaean metamorphism and minor intrusive rocks are limited to the Alanngua complex and its southern boundary zone with the Finnefeld complex.

## 5. Discussion

This integrated study has identified and characterised, in space and time, major crustal components of the Akia terrane and adjacent areas. Some possible implications of the results for the architecture, composition and evolution of the crust in this part of the NAC are discussed.

### 5.1. Age and nature of identified shear zones

The aeromagnetic data provides evidence for a network of shear zones. Comprehensive field and geochronological studies in the Nuuk area has indicated that Mesoarchaean terrane boundaries are extremely difficult to trace because they have undergone later deformation and have been partly obliterated or excised by Neoarchaean tectonic activity (e.g. Friend and Nutman, 2019). Thus, in view of the regional scale adopted, we do not expect to identify older terrane boundaries in the aeromagnetic image. One previously recognised Mesoarchaean shear or high strain zone, the Qugssuk-Ulamertoq zone (Fig. 2B, 4), is coeval with a granulite-facies metamorphism at ca. 2980 Ma and N-S striking tight folds (Garde, 1997). Otherwise, the indicated shear zones (Fig. 4) are

**Table 2**

Summary of observations and data for 12 areas or complexes within the study area.

Area	Tuno	Tuno keel	Alanngua	Qullugianngut	Isortoq	K-F zone	Four lakes	Finnefjeld	Taser-ssuaq	Fiskefjord	Nuup K	Late granitoids
<b>Lithology</b>	orthogn, msed, mafmv	orthogn msed	orthogn, msed, mafmv	orthogn, mafmv	orthogn, mafmv	orthogn, mafmv	orthogn, mafmv	orthogn	orthogn	orthogn, mafmv	orthogn, mafmv	granodio granite
<b>Metamorphic grade</b>	H (L)	H	H	H	H (L)	?	L	L (H)	L	H and L	L	L
<b>Metamorphic event (s) Ma</b>	3009, 2733	2816	2800–2500		2941?					3000–2980	3000–2980	
<b>Magnetic field intensity</b>	H and L	H	L (M)	H	H (L)	L and H	L	H and L	H	variable	L	L
<b>Direction of fold pattern</b>	variable	NNE	N-E	ENE-E	NE-E	NE	NNW	NE	weakN	N and convolute	N	N
<b>SS magn. fract.</b>	H and L	M	L	H to M	H	L	L few H	L	L	variable	L	L
<b>SS Ni content</b>	H to M	H to M	L to (H)	H to M	H	L	M to H	L	L	H to M	H	L
<b>SS Rb content</b>	H and L	L	H	L to M	L	variable	H	variable	variable	L to M	M to H	M
<b>No of rock samples</b>	4	5	20		26	24		84	34	184	16	31
<b>Perc. TTG s.s.*</b>	0	80	55		31	38		25	12	49	69	16
<b>Perc. &gt; 5% maf. index</b>	75	0	35		62	50		52	53	48	6	3
<b>Perc. K/Na &gt; 0.6</b>	25	20	10		8	13		23	35	2	25	81
<b>Perc Rb &gt; 30 ppm</b>	75	20	45		35	50		74	94	22	100	97
<b>Orthogneiss age<sup>#</sup> Ma</b>												
<b>3300–3100</b>			x							x		
<b>3100–3015</b>			x		x					x	x	
<b>3015–2990</b>		x	x	x	x	x		x	x	x		
<b>2990–2900</b>		x	x			(x)		x	x	x		x
<b>2900–2800</b>	x										x	
<b>2800–2700</b>	x		x									
<b>2700–2500</b>			x									

High metamorphic means granulite facies, low grade means amphibolite facies

Nuup K: Nuup Kangerlua

orthogn: orthogneiss

msed: metasedimentary rock

mafmv: mafic metavolcanic rock

SS: stream sediment

H:high

L:Low

M: Medium

() minor areas

No: number

Perc.: percentage

\* SiO<sub>2</sub> > 64%, mafic index (TiO<sub>2</sub> + Fe<sub>2</sub>O<sub>3</sub> + MnO + MgO) < 5%, K<sub>2</sub>O/Na<sub>2</sub>O < 0.6 (Moyen and Martin, 2012)<sup>#</sup>interpreted protolith age (Table 1)

undeformed or only weakly deformed and are probably Neoproterozoic or younger. Considering Neoproterozoic tectonism and metamorphism documented in the Nuuk region (Friend and Nutman, 2019), the shear zones have likely been reactivated after they first formed. The Ilivilik shear zone truncates and is younger than Finnefeld and Tasersuaq complexes (Fig. 2A). It has been ductilely deformed and hence is probably older than the latest Neoproterozoic deformation. The Kangia shear zone (Fig. 4) appears to have been active in the Neoproterozoic. Sample 218 of Finnefeld orthogneiss collected at the shore of Kangia fjord, within the shear zone, shows evidence for protracted zircon growth 2775–2708 Ma and sample 212 has ca. 2650 Ma metamorphic rims on zircon grains (Table 1; Section 4.4; Fig. 11 A, B).

Age relationships within the Kangia-Fossilik zone are complicated. Linear elements are dominantly Palaeoproterozoic dykes and faults, but these probably use an older crustal fabric, since two of the otherwise N–S directed BN dykes (Nilsson et al., 2013) have been accommodated in this zone. The initial structure could be Mesoproterozoic since it follows the southern limb of the large fold structure seen in the Isortoq high. The steep foliation in the same direction in the Finnefeld gneiss likely formed before or simultaneously with the Neoproterozoic shear zones.

Neoproterozoic reworking and metamorphism to granulite-facies grade was recognised by Kirkland et al. (2018) based on samples that are now recognised as components of the Alannua complex. Based on the now available aeromagnetic and zircon age data, it is evident that Neoproterozoic shearing affected the northern Akia region and the boundary zone between the Akia and Tuno terranes, while Neoproterozoic magmatism and metamorphism is so far only recorded in the boundary zones between the Akia terrane and Alannua complex.

The northern part of the ca. 2550 Ma Ivinnguit fault (Friend and Nutman, 2019) separates the strongly magnetic Tasersuaq complex from the weakly magnetic Isukasia terrane, while the southern part has weakly magnetic rocks on either side (Fig. 10). Instead, the abrupt contrast between strong and weak magnetic response runs along the east coast of Nordlandet where it marks a change from granulite in Nordlandet to amphibolite-facies east of the fjord Nuup Kangerlua. No tectonic feature has yet been suggested for this obvious linear and steep boundary, hidden by the fjord.

## 5.2. Cause of the magnetic highs and lows within the Akia terrane and Alannua complex

The variation in magnetic field intensity relates to the magnetic properties of the exposed rocks, and the principles in linking magnetic field variation to lithology is described by Clark (1999). The magnetic properties of outcropping rocks, such as magnetic susceptibility and content of magnetic minerals, are not available for the study area. However, Precambrian shield areas of Finland (Puranen, 1989; Grant, 1985; Clark, 1999; Airo and Säävuori, 2013), Canada (Ontario Geological Survey, 2001) indicate that orthogneiss with dioritic compositions generally has stronger magnetic response than more felsic rocks such as TTG gneiss. Mafic or ultramafic plutonic rocks may have high or low magnetic response depending on the proportion and nature of contained Fe-Ti oxides (Grant, 1985). Supracrustal mafic metavolcanic or meta-sedimentary rocks are usually poor in magnetic minerals and can thus, generally, be associated to magnetic lows, and likewise granodioritic and granitic orthogneiss. With increasing metamorphic grade, the susceptibility of an orthogneiss may increase due to recrystallisation of Fe-bearing silicate minerals and formation of secondary magnetite (Larsen, 1981; Grant, 1985; Olesen et al., 1991; Nielsen and Rasmussen, 2004). Hence, when using the aeromagnetic data to deduce the nature of the lithological cause of the anomalies, both chemical composition and metamorphic grade must be considered. The best indicator of the magnetic properties of outcropping rocks we have in the study area, is the magnetic mineral content of stream sediments (Fig. 6 A).

In the Alannua complex, the geochemistry of the rock samples indicates that dioritic rocks occur in the southern part where the magnetic

response is moderate (Fig. 4,7). In the northern part of the complex low contents of magnetic minerals and high Rb in stream sediment are consistent with low magnetic response and predominance of more evolved granodioritic to granitic orthogneiss. The complex was described as amphibolite-facies by Noe-Nyegaard and Ramberg (1961), however, Neoproterozoic granulite-facies metamorphism of metasedimentary rocks was documented in Kirkland et al. (2018). This suggests that the entire complex is high grade, and that the orthogneiss has such low concentration of mafic components that the formation of magnetite as well as hypersthene has been prevented (e.g. White et al., 2017). Alternatively, the low-magnetic and Rb-rich orthogneiss in the poorly known northern and eastern part of the complex (Fig. 6C, 8i) are younger than the high-grade metamorphism. More field work is warranted in the less investigated parts of the Alannua complex to assess this.

In the Akia terrane, a small but intense magnetic anomaly at the north-eastern edge of the Finnefeld complex (Fig. 1 A, 4) is readily explained by accumulation of magnetite in the Qaqarsuk carbonatite. The low magnetic response in Four Lakes and Nuup Kangerlua areas are spatially correlated with low content of magnetic minerals and high Rb in stream sediment and rocks (Fig. 6 A, C, 8 I) consistent with predominance of felsic orthogneiss at amphibolite-facies metamorphic grade. The prominent slivers of mafic metavolcanic rocks enclosing abundant bodies of ultramafic rocks confirms that such rock assemblages do not cause an increase in the magnetic response, however, they are reflected in the moderate to high Ni contents of stream sediment (Fig. 6B). The typically low magnetic intensity of the Fiskefjord complex is consistent with the predominance of felsic (tonalitic-trondhjemitic) retrogressed orthogneiss and metavolcanic rocks. The entire Fiskefjord complex is high-grade, but higher magnetic response areas are only correlated with bodies of dioritic orthogneiss. Mapped elongate bodies of metadiorite coincide with similarly shaped moderate magnetic highs. The metadiorite enclaves in Nordlandet are both dioritic (to gabbroic, Fig. 8c) and at high metamorphic grade and are a convincing cause of the moderate magnetic anomalies imitating their shapes (Fig. 4). In addition, the stream sediment data confirm elevated to high contents of magnetic minerals (Fig. 6A). However, the difference in magnetic response between metadiorites in the western part of Nordlandet and the eastern part, where the very strong anomaly (NE, Fig. 4) occurs, and stream sediment has lower content of magnetic minerals, is unexplained. In the northern part of the Akia terrane, the magnetic anomalies (I and Q) are associated with orthogneiss in granulite-facies, and the elevated to high content of magnetic minerals in stream sediment indicate that the outcropping rocks could be the cause of the magnetic response. A large proportion of the orthogneiss in the Isortoq high are dioritic in composition (Fig. 9, Table 2). However, the magnetic response from eastern Q area is very strong (>1000 nT, Fig. 2A) and the difference in magnetic intensity between Isortoq and eastern Qullugiannuit highs is also unexplained. Neither is it clear why the same kind of rock assemblage (orthogneiss and amphibolite) should cause higher magnetic response in the northern than in the southern part of the terrane (the Fiskefjord complex).

The tonalitic to granodioritic composition of most of the Tasersuaq complex is consistent with the low content of magnetic minerals in the sediment from streams draining the outcropping rocks. Thus, this rock is an unlikely cause of the large magnetic anomaly (T, Fig. 4). It is therefore probable that the anomaly is caused by rocks lying underneath the felsic rocks. The north-western part of the magnetic high extends beyond the Tasersuaq complex and this gives an opportunity to search for the cause of the high magnetic response. Fig. 12 shows a close-up of the 1:100,000 scale geological map of that area. Felsic orthogneiss dominates, but there is outcropping metadiorite and abundant inclusions of metadiorite in the felsic gneiss which can account for higher magnetic response. Rock samples from the area (Figs. 7, 8) confirm the presence of dioritic rocks. The two samples within this area are marked with triangular symbol in Fig. 7 and are plotted with K-F zone samples in

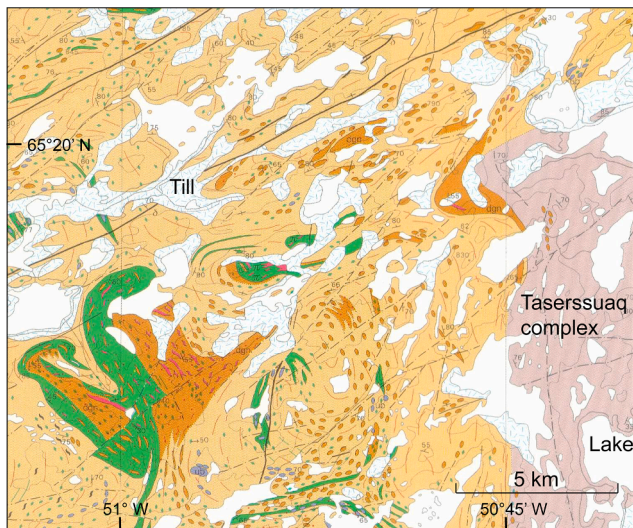


**Fig. 12.** Selected part of 1:100,000 scale geological map (Hall and Hughes (1982; Garde, 1987) covering an area within the aeromagnetic high (T, Fig. 4) north-west of the Taserussuaq complex. Outcropping metadiorite (in brown) and undifferentated orthogneiss (beige) with abundant inclusions of metadiorite indicating subsurface extent of metadiorite.

**Fig. 8.** The common occurrence of dioritic xenoliths in the felsic rocks of the Taserussuaq complex (Garde 1997) strengthens the evidence that dioritic, and perhaps also more mafic plutonic rocks, underlie the outcropping granodioritic rocks. The aeromagnetic data therefore indicates the presence of a large body of rock with a dioritic or more mafic composition beneath the felsic orthogneiss.

The much smaller aeromagnetic high (FS, Fig. 4), south of the Finnefjeld complex is not covered by a detailed geological map, but field observations in the area document the presence of dioritic orthogneiss (Fig. 13 A, B), as does the dioritic composition of samples from the same area (Fig. 9). Metadiorite xenoliths are also common in the Finnefjeld complex (Fig. 13 C), and a ca. 50 m wide body of metadiorite surrounded by felsic orthogneiss spatially coincides with a small high in the Finnefjeld complex (Figs. 4, 13 D). Rock samples with dioritic composition ( $\text{SiO}_2 < 64\%$  and mafic index  $> 5\%$ , Fig. 7) confirm the intermediate to mafic nature of rocks within areas of high magnetic response.

The magnetic intensity is variable to weak in the northern part of the Finnefjeld complex. The K-F zone with closely spaced NE-striking zones of strong ductile shearing and brittle deformation plus dolerite intrusion passes north of the Taserussuaq complex but right through the Finnefjeld complex north of the FinneS magnetic high. If a magnetic anomaly caused by underlying rocks did continue to the north, it would likely have been weakened or destroyed by alteration of magnetic minerals associated with the deformation. However, irrespective of a possible northerly extension of a buried more mafic unit, the Finnefjeld spectrum of rock chemistry from the entire outcrop area exhibits an affinity with a dioritic magma (Figs. 7, 8).

The simulation of the subsurface continuation of the magnetic field (Fig. 3) provides a hint to the cause of the strongest anomalies. The data indicate that these anomalies (Q, T, FS) possibly, (i.e. according to the concept behind the filter, Jacobsen, 1987), are caused by a source that continues to considerable depths ( $>15$  km), which implies that they could be associated with rocks of high susceptibility creating large vertical bodies. A likely option is a mantle-derived basic magma that has intruded into the crust of the Akia terrane. According to Grant (1985) and Clark (1999), low-Ti anhydrous plutonic rocks such as certain gabbros and norites may be strongly magnetic. An example is the Palaeoproterozoic Bushveld mafic-ultramafic complex in South Africa that has strong magnetic response (Letts et al., 2011).

In summary, moderate to strong magnetic highs are associated with

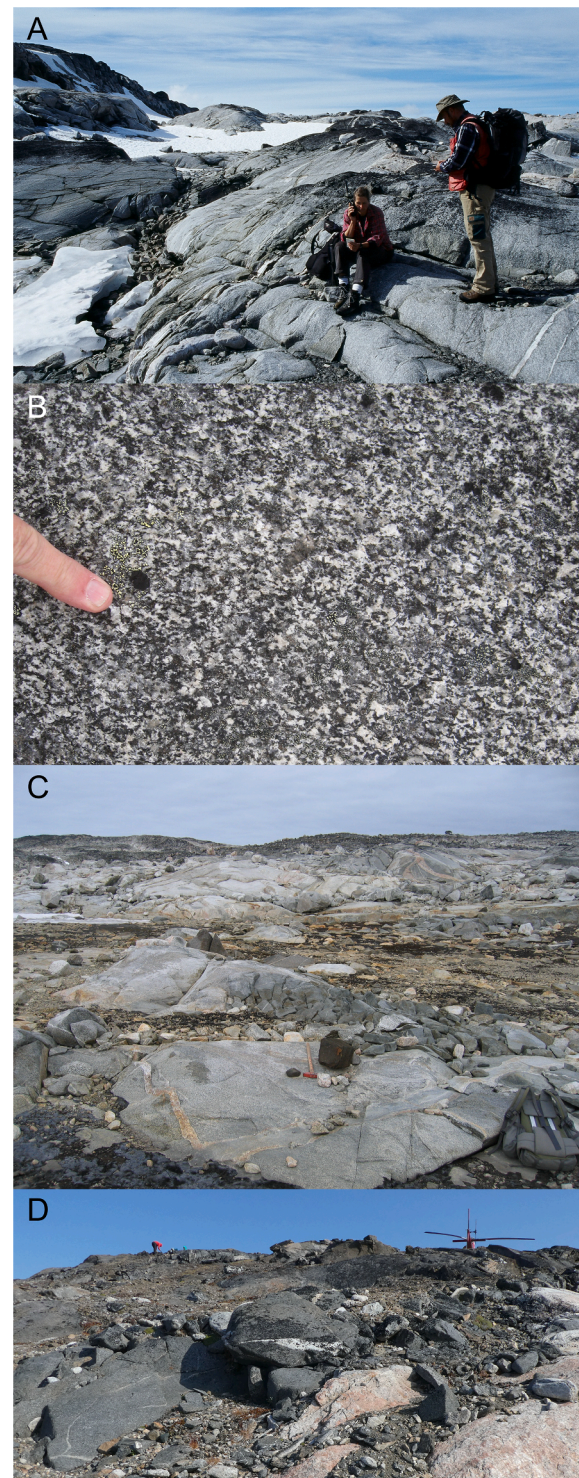


**Fig. 13.** A: Outcropping metadiorite in the 'Finne S' aeromagnetic high (Fig. 4). Photo by J. Keiding. B: Close-up of diorite outcropping in the 'FinneS high'. Photo by H. Stendal. C: View towards north-east in the Finnefjeld complex showing light grey orthogneiss with inclusions of darker metadiorite and later generations of granitic veins. Kimberlite float and rucksack in the foreground and dark, crumbly weathering metanorite in the background. Photo by K. Secher. D: Large metadiorite body flanked by pegmatite exposed in the centre of the Finnefjeld complex. Partly hidden helicopter against the sky in the background. Photo by H. Heide-Jørgensen. Locations in Fig. 4.

dioritic/mafic orthogneiss metamorphosed at granulite-grade conditions. However, the strongest magnetic response within those highs needs a contribution from another source to be explained, and that contribution is proposed here to be one or more of large subsurface bodies of mafic rocks with an upper zone of partly outcropping diorite. Outcropping bodies of metagabbro enclosed by felsic orthogneiss occur within a 5x5 km large area at the strongest southern anomaly of the Taserssuaq complex (Chadwick and Coe, 1988; Fig. 4) support the presence of gabbroic in addition to dioritic rocks.

### 5.3. Timing and spatial distribution of magmatism and metamorphism

Zircon geochronology as grouped by area (Table 2; Figs. 10 and 11) reveals spatial differences in the timing of both magmatic and metamorphic events.

#### 5.3.1. Magmatism

Traces of Eo-Palaeoarchaeon enclaves within the study area are confined to the Alannua complex, where Eoarchaeon zircon grains are found in orthogneiss from the easternmost part (Qarliit Tasersuat; Nutman et al. 2004), and Palaeoarchaeon ages were recently identified in xenocrystic zircon crystals hosted by a kimberlite in the south-western Alannua complex, close to sample 316 in Fig. 10 (Gardiner et al., 2020). The Tuno terrane north of the study area encloses the small proposed Eoarchaeon Aasivik terrane, ca. 60 km north of Majoqqaq (Rosing et al., 2001), however, no magmatic rock ages of > 3300 Ma have been recorded within the Akia terrane.

Late Palaeoarchaeon to early Mesoarchaeon rocks are recorded in the Fiskefjord complex – the 3240–3180 Ma Nordlandet metadiorite and a small metadiorite xenolith in metatonalite (Gardiner et al., 2019). In the Alannua complex, sample 316 of orthogneiss has a component of similar age, and xenocrystic zircons of this age range occur in other samples from the Alannua orthogneiss as well as in a few detrital zircon grains from metasedimentary rocks in the complex (Table 1, Fig. 11C). A sample from Qarliit Tasersuat has two zircon ages in the 3300–3100 Ma interval, and noticeably a granulite-facies orthogneiss sample collected south of the Aasivik terrane has 10 magmatic zircon dates in two age groups, 3226–3198 Ma and 3134–3131 Ma (Rosing et al., 2001). This age interval is not represented in samples from Isortoq, K-F zone, Finnefeld and Taserssuaq complexes apart from one analysis within a xenocrystic zircon from the K-F zone yielding an age of 3225 Ma (Table 1; Olierook et al., 2020).

The next age interval (3100–3015 Ma, Figs. 10, 11, Tables 1, 2) prevails in the southern part of the Akia Terrane, where such ages have been interpreted to represent formation of a volcanic arc at ca. 3070 Ma and magmatic accretion of orthogneiss precursors 3060–3016 Ma (summary in Garde et al., 2014). However, in the Alannua complex, orthogneiss (samples 316, 541) and detrital zircons in metasedimentary rocks record the same age interval (Fig. 11 C). The Isortoq area has one orthogneiss sample dated at ca. 3035 Ma (Scherstén and Garde, 2013) and xenocrysts with ages between 3100 and 3015 Ma occur in rocks from other areas (Table 1; Olierook et al., 2020). It therefore seems likely that the 3070–3015 Ma crust represented by the Fiskefjord complex covers a large area into which the plutonic complexes of the subsequent magmatic events were emplaced.

A significant amount of plutonic rocks was added to the crust in the period 3015–2990 Ma. Gardiner et al. (2019) documented that orthogneiss with such zircon ages prevail within and in the surroundings of the Finnefeld complex. The present compilation shows that such ages are also seen in zircon crystals from the Taserssuaq complex and in almost all orthogneiss samples from the northern Akia terrane (Qullugiannuit, Isortoq and K-F zone, Fig. 10) as well as in samples from the Alannua complex and Tuno keel (Table 1, Figs. 10–11; Garde et al., 2000; Gardiner et al., 2019; Scherstén and Garde, 2013). (Table 1, Fig. 11). In the southern Taserssuaq complex, a  $3006 \pm 6$  Ma hornblende diorite (sample 477307, Table 1; Hollis, 2005) ascertains that the dioritic

component, spatially associated with the Finnefeld and Taserssuaq complexes, was part of the same magmatic event. This is further supported by the observation that most samples from this age group occur within aeromagnetic highs (Fig. 10; section 5.2). Sample 212 and 213 are both coarse-grained hornblende-bearing rocks with lesser medium grained dioritic enclaves from the Finnefeld complex and their interpreted magmatic zircon ages (ca. 2986 and ca. 2987 Ma) are close to the 3015–2990 Ma age group and they likely represent a late phase of the Finnefeld complex. Recently acquired U-Pb zircon age data documents that the protoliths of the Maniitsoq Norite Belt (Fig. 1 A) intruded into the crust between 3013 and 3001 Ma (Waterton et al., 2020).

The 2990–2900 Ma age interval has been assigned to a period of deformation and crustal melting, the latter manifested by ca. 2975 Ma granitoid intrusions (Fig. 10) together with pegmatites and neosome formation in the north-western part of the Fiskefjord complex (Hall and Hughes, 1982; Garde, 2007). Grey granodiorite dykes dated at 2980–2970 Ma were emplaced in the same period (sample 896 and Olierook et al., 2020) and granitoid sheets of this age occur elsewhere within the Fiskefjord complex (red symbols in Fig. 10, red reference line in Fig. 11). The granitic and granodioritic sheets and dykes are clearly intrusive with sharp boundaries towards their host rocks and, together with coeval intrusive bodies that created brecciation during their intrusion suggest these magmas were emplaced into relatively colder brittle rocks during tectonic activity. Sub-solidus recrystallisation, metamorphic overgrowth or neoblastic zircon growth at 2990–2900 Ma is coeval with anatectic melting of existing crust. The reworking and melting of felsic crust have been interpreted as resulting from crustal shortening (Garde, 2007). The Akia terrane could, therefore, be part of a collisional orogeny indicated by ca. 2970 Ma magmatism and metamorphism within the Nuuk terrane assemblage (Nutman et al., 2015).

Late Mesoarchaeon (2900 to 2800 Ma) igneous zircons have been identified in the Tuno terrane and border zone towards the Nuuk terrane assemblage (Table 1, Figs. 10, 11; Hollis, 2005; Kirkland et al., 2018). Neoarchaeon 2800–2700 Ma magmatic ages are seen locally in the Alannua complex, where two pegmatites are dated at 2729 Ma (Gardiner et al., 2019). The latest Neoarchaeon magmatic age, ca. 2558 Ma, is recorded in a granite sheet in the Finnefeld complex, adjacent to the Alannua complex. Otherwise, Neoarchaeon ages in Fig. 11A–B are interpreted as metamorphic.

#### 5.3.2. Metamorphism

Zircon evidence for metamorphism in the period 3000–2980 Ma is recorded from throughout the Akia terrane, the Alannua complex, and in Akia-aged enclaves within the Tuno terrane. Metabasalt and metaandesite with ca. 3070 Ma depositional age in Nuup Kangerlua-Qussuk areas show metamorphic ages from shortly after 3000 Ma onwards and culminating with sillimanite-grade amphibolites-facies ca. 2980 Ma and mobilization of granite at around 2975 Ma (Hollis, 2005; Garde et al., 2012c). This thermal event is coupled with a period of crustal reworking and intrusion of anatectic granitoid melts referred to above (Garde, 2007). Two granulite-facies metamorphic events, 3000 and 2980 Ma, are stated for the southern Akia terrane in Friend and Nutman (2019); granulite-facies metamorphism was dated in a rare occurrence of metasedimentary rock in Nordlandet at ca. 2999 Ma (Friend and Nutman, 1994) and at ca. 2981 Ma in a tonalitic orthogneiss further north in western Fiskefjord complex, regarded as the peak of metamorphism (Garde et al., 2000). However, the number of ages between 3000 and 2950 Ma recorded in samples of presumed anatectic melts from the Fiskefjord complex (between blue and red lines in Fig. 11 B) suggest that high grade metamorphic conditions and associated anatectic melting lasted throughout this age interval in this part of the Akia terrane. The orthogneiss of the Isortoq area has granulite-facies mineralogy and metamorphic ages at ca. 2980 Ma (A.P. Nutman, pers. comm., 2020) in addition to the uncertain age of ca. 2941 Ma in sample G94/3 (Table 1), but no high-grade metamorphism older than 2980 Ma is recorded by the zircons in this area. Yakymchuk et al. (2020) determined high T

granulite metamorphism at 3009 Ma in a sample from the Tuno terrane (740, Table 1), inferred to be part of an enclave of the Akia terrane within younger Tuno terrane gneisses, and 2989 Ma metamorphic age in granulite-facies leucosome within an amphibolite from the Alannua complex.

The Rb concentration of orthogneiss is a useful indicator of the intensity of high-grade metamorphism, because Rb is depleted during recrystallisation and removal of anatectic melts during high-grade metamorphism as shown by Garde (1990). Thus, the granulite-facies orthogneiss of the Fiskefjord complex (Fig. 8k) has the lowest Rb concentrations but such low contents are also seen amongst granulites from the Isortoq area and some samples from Tuno, and Alannua areas (8i). Rb in stream sediments confirm a spatial distribution of low Rb in the south-western Fiskefjord complex and Isortoq area and indicates that the high-grade conditions also prevailed in the Qullugiannuit area. The high Rb seen in Nuup Kangerlua and Four Lakes areas is consistent with lower metamorphic grade in these areas (Fig. 6C, 8 l).

Thus, while high temperature granulite-facies conditions (>800° and < 0.9 GPa, Riciputi et al., 1990; Yakymchuk et al., 2020) were attained in the western Fiskefjord complex and also at this time in the southern Alannua complex, the south-eastern part and Four Lakes areas reached only amphibolite-facies. Garde (2007) ascribes the geographic difference in metamorphic grade to eastwards tilting of the crustal block hosting the Akia terrane whereby presumed lower crustal levels became exposed in the west. Such tilting could be driven by uplift prior to the Mesozoic opening of the Labrador Sea (Larsen et al., 2009). Widespread retrogression of granulite-facies orthogneiss in the Fiskefjord area took place after the high-grade metamorphism and before the intrusion of the ca. 2975 Ma Qussuk granite, but the timing of this event is apparently not reflected in zircon U-Pb data (Garde 1990; Garde et al., 2000).

The Finnefeld and Tasersuaq complexes were emplaced during peak metamorphism and onset of crustal reworking. Contemporaneous metamorphic overgrowth has not been recorded in the zircon populations compiled here (Fig. 11 A, B), but relict orthopyroxene has been reported in mafic enclaves of the Finnefeld complex (Berthelsen, 1962). The high percentage (>70%) of samples with Rb > 30 ppm indicates that the Finnefeld and Tasersuaq orthogneiss apparently did not suffer Rb loss. Both complexes have mineralogical signs of retrogression, and fluid-present amphibolite-facies conditions for this was indicated by mineral paragenesis in samples from the Tasersuaq complex (Garde et al., 1986; Garde, 1997).

Late Mesoproterozoic to Neoproterozoic granulite-facies metamorphic conditions (Table 1, Fig. 11 C) were reached in the Alannua complex at 2857–2700 Ma, where temperatures of ~820–850 °C at 8–10 kbar have been established (Kirkland et al., 2018). This younger granulite-facies event was at higher pressure than during the 3000–2980 Ma event. In the Alannua complex, low values in some rock and stream sediment samples from the southern part likely indicate Rb-depletion during metamorphism. The low T-high P metamorphism in the Alannua complex is synchronous with high T-low P metamorphism in the Tuno terrane (Kirkland et al., 2018; Friend and Nutman, 1994).

Neoproterozoic metamorphic ages are not recorded in the Akia terrane except in two samples of Finnefeld orthogneiss adjacent to the Kangia shear zone (location in Fig. 10). Sample 212 provides evidence for 2650 ± 38 Ma metamorphic overprint and sample 218 of highly strained Finnefeld orthogneiss with broken zircon grains (Fig. 9), located close to the junction of the Kangia and Majoqqaq-Alannua shear zones, yield ages between 2775 and 2708 Ma consistent with protracted or recurrent Neoproterozoic reworking. The youngest Neoproterozoic metamorphic zircon ages (2600–2500 Ma) are recorded in metasedimentary rocks from the Alannua complex (Fig. 11C; Garde et al., 2000; Dyck et al., 2015).

#### 5.4. The Alannua complex and the boundary towards the Tuno terrane

The Alannua complex is a crustal segment that separates the Akia

and Tuno terranes. We have shown, that the complex is distinct from its bounding terranes, as it hosts most of the Neoproterozoic magmatic, metamorphic and tectonic activity known in the area. Its boundaries are defined here by the aeromagnetic lineaments that coincide with lithological boundaries drawn by Noe-Nygaard and Ramberg, 1961 and Berthelsen (1962).

In the area between the Alannua and Finnefeld complexes, the lineament is not so precisely defined in that the magnetically negative feature is wider (Fig. 2A, 4). This could indicate that the boundary is inclined in agreement with the structural interpretation by Berthelsen (1962) that the Finnefeld complex has been thrust north-westwards over the Alannua complex. In addition, the pattern of negative magnetic lineaments suggests the confluence of two sub-parallel shear zones in the western third of the Majoqqaq-Alannua zone. West of the Kangerluarsuk shear zone, the small peninsula, here termed Tuno keel, is characterised by a magnetic high that appears to continue northwards beyond the map limit between the Kangerluarsuk shear zone and the Aujassoq shear zone (Fig. 4). Two orthogneiss samples from the Tuno keel share their early zircon age dates with the Akia terrane, while they show < 2960 Ma metamorphic zircon growth like in the Alannua complex (sample 250, Table 1; Kirkland et al., 2018). The position of this small crustal segment in the crustal configuration pattern remains to be determined, and the boundary towards the Tuno terrane is still not sufficiently documented. We have tentatively placed the boundary along the Aujassoq shear zone (Figs. 1, 4).

Evidenced by the compiled and new zircon U-Pb dates, the history of the rocks within Alannua complex spans several hundred Myr. Detrital zircons indicate source regions with age ranges corresponding to the three age groups, 3300–3100, 3100–3015 and 3015–2990 Ma, found within the Akia terrane (Fig. 11 C), and the age spectrum of orthogneiss samples confirm the presence of such rocks within the Alannua complex itself (Figs. 10, 11A). It therefore looks as if the Alannua complex has a “basement” of Akia-aged rocks that is tectonically overlain by or interleaved with metasedimentary rocks having additional ≤ 2877 Ma to ≥ 2857 Ma source material, presumably derived from the Tuno terrane (Kirkland et al., 2018). However, while these authors assumed that the young supracrustal sequences prevailed over the entire Akia terrane, our presently compiled data show that the late Mesoproterozoic and Neoproterozoic ages are largely confined to the Alannua complex and Tuno terrane.

In their review of the architecture and evolution in the Nuuk region, Friend and Nutman (2019) recognised six episodes of post-2960 Ma magmatic and tectonic activity and related them to the separation and (re)assembly of the terranes within the Nuuk terrane assemblage. The Neoproterozoic ages within the Alannua complex are broadly coeval with those recorded in the Nuuk terrane assemblage and the complex could, therefore, have taken part of the same gross rearrangements of continental fragments, i.e. the Alannua complex was separated from the Akia terrane for a while and was re-assembled with the Akia and Tuno terranes during the Neoproterozoic. For example, the youngest identified event evidenced by metamorphic zircons at the Kangerluarsuk shear zone at the western boundary of the Alannua complex were dated at ca. 2558 Ma (Garde et al., 2000; Dyck et al., 2015), thus coeval with the Ivinnguit fault (Friend and Nutman, 2019), (Fig. 1). The Tuno keel with an orthogneiss age common to the Akia terrane suggests it may be part of the tectonically disturbed boundary zone instead of being a part of the Tuno terrane.

The observations and obtained data document that the Alannua complex may be described as a Neoproterozoic tectonic melange created by recurrent reworking during high-grade metamorphism (~820–850 °C and 8–10 kbar). It will, however, require more studies and dedicated field work to separate the tectonic events and create a reliable tectonic model for the complex.

5.5. Composition and generation of Mesoarchaeoan crust-forming felsic and intermediate plutonic rocks

The large number of analysed samples has enabled geochemical characterisation of the main components of the Akia terrane, identified some significant differences across the terrane, and have implications for the proposed models for crust generation.

Archaean crust is often described as composed largely of TTG (orthogneiss with tonalite-trondjemite-granodiorite composition), and Archaean felsic to intermediate orthogneiss is commonly referred to as TTG in the literature, often without litho-chemical data to sustain that the orthogneiss may be classified as TTG (Moyen, 2011; Moyen and Martin, 2012). However, although TTG suite rocks are certainly present in the Akia terrane, they cannot be said to predominate according to the litho-chemical data in our compilation where we used three main criteria proposed by Moyen and Martin (2012) to define TTG s.s. (section 4.3; Figs. 7–8, Table 2). In fact, 48 to 62% of the samples of crust-forming rocks within the Akia terrane are more mafic than typical TTG, i.e. with a “mafic index”,  $(\text{TiO}_2 + \text{Fe}_2\text{O}_3 + \text{MnO} + \text{MgO})$ , > 5 and up to 20%. Excluding the samples of the ca. 3220 Ma Nordlandet metadioritic gneiss from the calculation increases the percentage of TTG s.s. in the

remaining 3050–3020 Ma Fiskefjord complex to 56%, which is still not very high. Within each area, the smallest fraction of the samples is granodioritic to granitic in composition ( $\text{K}/\text{Na} > 0.6$ ; Fig. 7). Thus, the Mesoarchaeoan crust of the Akia terrane is not largely TTG. The implication of this finding is that any proposed model for the generation of the Mesoarchaeoan crust of the Akia terrane should be able to account for the generation of an appreciable amount of dioritic rocks, not just TTG.

It is generally agreed that the Archaean TTG is produced by partial melting of hydrated mafic crust, although the geodynamical setting for this mafic crust is still debated (review by e.g. Arndt, 2013; Hawkesworth et al., 2017; Hastie and Fitton, 2019). The concentration of Yb and the ratio  $\text{La}/\text{Yb}$  in sodic tonalitic rocks (belonging to the TTG series of Archaean felsic orthogneiss) has been widely used to assign a pressure regime for the melting (see reviews by Halla, 2018 and Moyen, 2011). TTGs were divided into light rare earth element (LREE)- and heavy rare earth element (HREE) types corresponding to high-pressure (HP) and low-pressure (LP) melting conditions, respectively, based on the concept that at high pressures, garnet in the melt zone would retain HREE. This concept was also used by Gardiner et al. (2019) to interpret chemical differences between the Finnefjeld and other orthogneiss units (15 samples in total) as derived by different depths of melting of a common

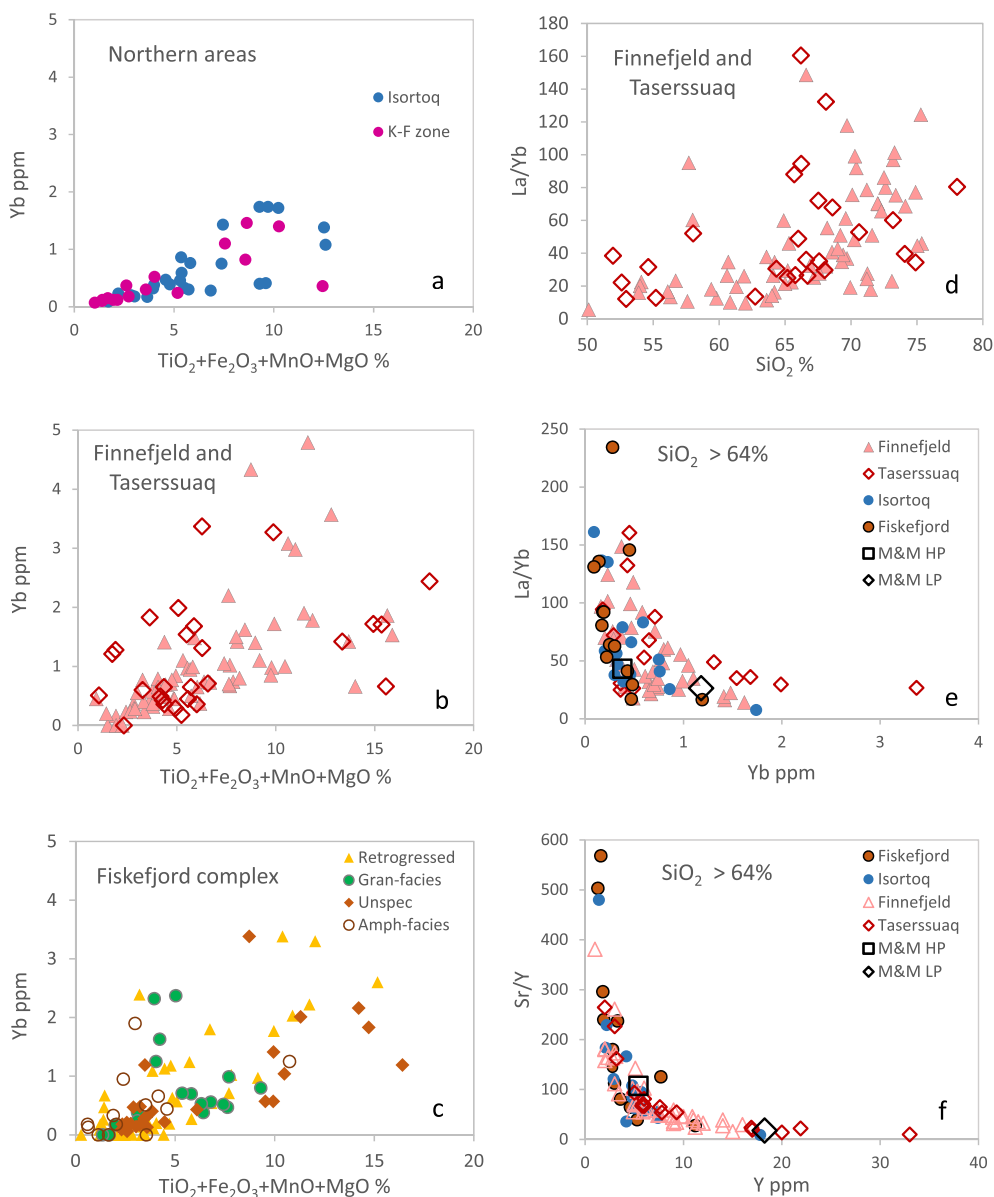


Fig. 14. Yb behaviour in rocks of the Akia terrane. Left panel: Yb increases with increasing mafic index in rock samples from all areas, compare Fig. 7. Note the scatter that must be taken into account when using Yb of this dataset for petrogenetic modelling. Right panel: d: variation of  $\text{La}/\text{Yb}$  in samples from Finnefjeld and Taserssuaq complexes showing correlated behaviour of Yb and  $\text{SiO}_2$ . e-f: Yb-La/Yb and Y-Sr/Y systematics for samples with > 64%  $\text{SiO}_2$ . Symbols for average high-pressure (HP with low HREE) and low-pressure (LP, high HREE) sodic TTG (Moyen and Martin, 2012) are shown for comparison.

pile of mafic crust.

Here, we assess 84 samples from the Finnefjeld, 34 from the Taserssuaq complex and 226 samples of prevailing orthogneiss from the remaining Akia terrane. The orthogneiss populations from all areas indicate that HREE, represented by Yb, are correlated with the mafic index, and that La/Yb correlates with SiO<sub>2</sub> (Fig. 14 a–d). Thus, by partial melting of amphibolite, a larger degree of melting will lead to more mafic melts with higher Yb and Y and this might be misinterpreted as lower pressure melting. Likewise, depletion in Yb and Y could be accomplished by crystal fractionation of a tonalitic magma and the more siliceous differentiates, trondhjemite and granodiorite, might be misinterpreted to have formed at higher pressure. The diagrams also show the considerable scatter in Yb values which is ascribed to a combined effect of irregular distribution of host minerals such as hornblende (Arth and Barker, 1976) in the medium to coarse grained rocks and low analytical precision at low Yb.

Another complication is that the granulite-facies orthogneiss of the Fiskefjord complex cannot be assumed to represent the melt composition. The high T metamorphism involved partial melting, whereby granitic melt and possibly fluids was removed from the original rocks (Garde, 1990). This is indicated by the lower Rb and K<sub>2</sub>O/Na<sub>2</sub>O in granulite-facies than in amphibolite-facies rocks of the Fiskefjord complex (Fig. 8 k, l). Removal of a granitic component would increase the amounts of mafic components together with Y and Yb. Hence, the use of HREE or Yb concentration as a pressure indicator may be misleading if applied uncritically to the orthogneiss of the Akia terrane.

#### 5.5.1. The Finnefjeld and Taserssuaq complexes

It has long been recognised that the Finnefjeld and Taserssuaq plutonic complexes are similar in appearance, mineralogy, chemical composition and younger age relative to the 3050–3030 Ma Fiskefjord tonalitic orthogneiss (Hall, 1984; Garde, 1997), and the two plutons have been interpreted as late stages of subduction-related magmatism (Garde 1997, 2007). Later, the Finnefjeld complex was proposed to result from a  $\geq 3000$  Ma meteorite impact (Scherstén and Garde, 2013). Later again, based on more zircon U-Pb ages, Lu-Hf isotopic and whole-rock chemical data, the Finnefjeld complex together with surrounding tonalitic orthogneiss were interpreted to represent melting of mafic crust at various depths (Gardiner et al., 2019). The latter papers did not concern the Taserssuaq complex.

When discussing the origin of the protolith magma for the Finnefjeld and Taserssuaq complexes it is important to look at the compositional variation of the entire rock suite – not just samples with TTG-like geochemistry, which in the Akia region are in the minority. The problem with the melting of mafic crust is that it does not account for the, on average, more mafic and at the same time more potassic composition of the Finnefjeld complex relative to that of the coeval surrounding orthogneiss (Gardiner et al., 2019). A larger degree of melting of a mafic source could account for the increased mafic component of the melt, however, that would at the same time reduce the concentration of K in the melt, in conflict with the higher K concentration observed in the Finnefjeld complex.

The La/Yb-Yb and Sr/Y-Y diagrams further illustrate that the Finnefjeld and Taserssuaq complexes are different from TTG and cannot be accounted for using common models for sodic TTG formation (Moyen and Martin, 2012). The diagrams (Fig. 14 e-f) are based on analytical data for samples with  $>64$  wt% silica, to comply with Archaean TTG suites usually displayed in such diagrams (e.g. Moyen, 2011, and Gardiner et al., 2019). The Finnefjeld and Taserssuaq suites cover the entire range from high La/Yb-low Yb to low La/Yb-high Yb, and equally high Sr/Y-low Y to low Sr/Y-high Y. Thus, the suite resembles neither Archaean high-pressure TTG (along Y-axis) nor modern continental crust or low-pressure TTG (along X-axis). The position of average high-HREE and low-HREE of Moyen and Martin (2012) is shown as reference.

Coupling the Finnefjeld and Taserssuaq complexes with a large gabbroic rock volume opens the possibility that the protolith of the

quartz dioritic and dioritic orthogneiss could represent the differentiated upper part of a gabbroic magma like, for example, the hornblende quartz monzonites of the roof zone of the Bushveld complex (Cawthorn, 2013).

#### 5.5.2. Towards a broader scenario for the 3015–2990 Ma event

The synchronous production of a broad compositional suite of rocks, i.e. noritic, carbonatitic, dioritic-granodioritic and tonalitic-trondhjemitic rocks was closely followed by high-temperature, low-pressure metamorphism (Bizzarro et al., 2002; Gardiner et al., 2019; Yakymchuk et al., 2020; Waterton et al., 2020). We consider a scenario where the required heat for the melting could be accomplished by asthenospheric upwelling, however, not as a protracted event (c.  $> 3.02$ – $2.98$  Ga) as suggested by Yakymchuk et al. (2020), but occurring after the formation of the Fiskefjord complex, i.e. at ca. 3015 Ma. Melting of lithospheric mantle could produce a voluminous ultramafic to mafic magma, which would act as a parent magma for both the metanorite and the metadiorite - granodiorite of the Finnefjeld and Taserssuaq complexes. The existing crust, the Fiskefjord complex and potentially underlying Eoarchaean root (Gardiner et al., 2020), exposed to heat from either the asthenosphere or the intrusion of large volumes of mafic magma, or both, could melt to form the coeval tonalitic-trondhjemitic orthogneiss and be responsible for the high-T metamorphism that has affected the entire Akia terrane. HF-isotope and trace element characteristics of the metanorites are consistent with a high degree of crustal contamination (Waterton et al., 2020). Likewise, the slightly negative  $\epsilon_{\text{Hf}}$  of zircons from the Finnefjeld orthogneiss (Gardiner et al., 2019) is consistent with incorporation of Eoarchaean crust into a fractionating gabbroic magma. Finally, the formation of the ca. 3007 Ma carbonatite can be explained by located melting of metasomatised lithospheric mantle (Bizzarro et al., 2002).

It likely that the cooling of the magmatic complexes had not yet come to an end when the uplifted Akia terrane was stirred by ductile and brittle deformation and local generation of crustal melts in the period 2980–2960 Ma, when a combined Akia-Kapisilik terrane is suggested to have collided with the Eoarchaean Isukasia terrane of the Nuuk terrane assemblage (see Nutman et al., 2015).

#### 5.5.3. The formation of the 3300–3015 Ma crust

The crust formed before the 3015–2990 Ma event may well have formed in other tectonic settings than that proposed above. No setting has yet been proposed for the 3240–3180 Ma scarcely studied dioritic crust incorporated into the Fiskefjord complex. The 3070–3050 Ma juvenile basaltic-andesitic metavolcanic rocks of the Nuup Kangerluqussuk area has been related to subduction (Garde, 2007; Szilas et al., 2015). The tonalitic magmas of the 3050–3020 Ma Fiskefjord complex were emplaced into tholeiitic crust during a compressional regime, have REE fractionation pattern typical of TTG, and have been interpreted to result from slab melting during subduction in a convergent margin (Garde, 1997, 2007), consistent with the model for generation of Archaean TTG by Martin (1994). However, as pointed out here, to generate the more basic magmas, a modern subduction model with additional melting of an overlying mantle wedge or another setting with access to mantle-derived melts is needed (Steenfelt et al., 2005a; review by Halla, 2018). Various models involving more complex interactions between mantle and crust have been developed for synchronous production of Archaean tonalite and diorite in other parts of the world (e.g. Käpyaho, 2006; Hoffmann et al., 2016; Laurent et al., 2020), however, further discussion of such models is beyond the scope of the present paper.

#### 5.6. The lack of evidence for a Mesoarchaean impact structure

Garde et al., 2012a; Garde et al., 2014 and references therein proposed that the Akia terrane hosts the roots of a  $>100$  km wide crater produced by meteoric impact  $\geq 3000$  Ma, the Maniitsoq structure. The

Finnefeld orthogneiss complex (35–50 km across) was seen as the impact centre, where deep-seated rocks were proposed to have been crushed and homogenized, while the surrounding area was envisaged to have suffered intense hydrothermal alteration. The evidence for the size and location of the Maniitsoq structure was based largely on aeromagnetic data (Garde et al., 2012a). Geological map units and a semi-circular zone of low magnetic response were described to curve round the Finnefeld complex (Garde et al., 2012a). Our analysis of the aeromagnetic data demonstrates the predominance of N-S or NE striking structures and we fail to recognise curved patterns centred on this complex (Figs. 2, 4) in accord with Reimold et al. (2013). The Finnefeld complex is not homogeneous but a polyphase complex (Fig. 13 C) with a large compositional variation (Figs. 8, 14) that has been deformed, metamorphosed, and transected by shear zones and faults (Figs. 1, 2). Garde et al. (2014) argued that observed crushing of rocks was caused by the impact, and they characterised post-impact deformation as localised, but Fig. 2 B demonstrates the regional character of the Kangia-Fossilik zone. Many of the observations of cataclastic rocks and brecciation reported by Garde and co-workers and are from within this zone. However, the possibility that the observed ‘cataclasis’ could result from Neo- or post-Archaean tectonic events like dyke intrusion, faulting, brecciation, and mylonitisation, as is widely recognised in the region, was not addressed by Garde et al. (2014). The chemistry of the Finnefeld complex was argued to be consistent with total melting of the ambient crust at the site (Garde et al. 2014), but this cannot be reconciled with the probable genetic link to the coeval and lithologically and chemically similar Tasersuaq complex, indicated previously and in the present work.

## 6. Conclusions

The compilation and integration of newly acquired together with previously published geological, geophysical, geochemical and geochronological data has provided an overview of available data which may serve as a framework for future research in the northern part of the North Atlantic Craton. During our study of the data, we have gained new insights in the architecture and evolution of the Akia terrane which we have presented here. Thus, the geochemical data allowed a preliminary evaluation of the crustal components within the study area and the geochronological data combined with field evidence for relative ages between rock complexes allowed an improved assessment of the crustal evolution. However, we point out that there are still poorly studied areas within the north-eastern Akia terrane, and there is a need for further field observations and acquisition of high-quality trace element and isotopic data in order to test and improve the interpretations made in this work.

In summary, our study has resulted in the following new recognitions:

- 1) The Alanngua complex is a Neoproterozoic tectonic melange situated between the Akia and Tuno terranes. Eoarchaean remnants and late Mesoproterozoic magmatic rocks are shared with the Tuno terrane and Mesoproterozoic magmatic rocks are shared with the Akia terrane. Neoproterozoic magmatic and metamorphic ages are largely absent in the Akia terrane.
- 2) The Mesoproterozoic crust within the Akia terrane is not largely TTG but has a high proportion of mafic orthogneiss. This has implications for modelling of crustal generation.
- 3) The 3015–2990 Ma dioritic-granodioritic Finnefeld and Tasersuaq complexes are chemically distinct from tonalitic-trondhjemitic orthogneiss elsewhere in the Akia terrane. They are spatially associated with areas of strong magnetic response inferred to be caused by large subsurface volumes of gabbroic-dioritic rocks. Carbonatite, high-Mg norite and tonalite-trondhjemitite were formed at same time, and we propose that this wide spectrum of rocks have formed by lithospheric and crustal melting in response to asthenospheric upwelling.
- 4) The crust-building episodes in the Akia terrane are previously

stated at ca. 3220–3180 Ma and 3070–2970 Ma. The latter may now be subdivided into volcanism at ca. 3070–3050 Ma, tonalitic and dioritic plutonism at ca. 3050–3020 Ma, gabbroic-dioritic-granodioritic plus tonalitic-trondhjemitic plutonism at ca. 3020–2980 Ma, and minor granitoid magmatism 2990–2940 Ma granitoid.

5) The present data analysis finds no support for the impact model (Garde et al., 2014 and references therein) for the generation of the Finnefeld complex.

## Declaration of Competing Interest

The authors declare that they have no known competing financial interests or personal relationships that could have appeared to influence the work reported in this paper.

## Acknowledgement

This work draws on field work, sample collection and geochemical data provisioned by the Ministry of Mineral Resources, Government of Greenland. We also wish to acknowledge the comprehensive documentation of field observations published in bulletins, reports and maps by The Geological Survey of Denmark and Greenland. S. M. Jensen and K. Secher are thanked for supplying photos. We are grateful for constructive criticism given by two anonymous reviewers and the helpful editorial handling by Martin Whitehouse. NJG thanks Australian Research Council grant FL160100168 for financial support.

## Appendix A. Supplementary data

Supplementary data to this article can be found online at <https://doi.org/10.1016/j.precamres.2020.105958>.

## References

- Aarestrup, E., Jørgensen, T.R.C., Armitage, P.E.B., Christiansen, O., Szilas, K., 2020. The Mesoproterozoic Amikooq Layered Complex of SW Greenland: Part I. Constraints on the P-T evolution from igneous, metasomatic and metamorphic amphiboles. *Mineral. Mag.*, mgm.2020.68
- Airo, M.-L., 2002. Aeromagnetic and aeroradiometric response to hydrothermal alteration. *Surveys in Geophysics* 23, 273–302.
- Airo, M.-L., Säävuori, H., 2013. Petrophysical characteristics of Finnish bedrock – Concise handbook on the physical parameters of bedrock. Geological Survey of Finland, Report of Investigation 205, 33 pp.
- Allaart, J.H., 1982. Geologisk kort over Grønland, 1:500 000, Sheet 2 Frederikshåb Isblink - Søndre Strømfjord. Grønlands Geologiske Undersøgelse, Copenhagen.
- Allaart, J.H., Jensen, S.B., 1979. Compilation of 1:500 000 reconnaissance mapping in the Precambrian of the Evighedsfjord - Søndre Strømfjord - Itivleq region, southern West Greenland. Rapport Grønlands Geologiske Undersøgelse 95, 72–76.
- Allaart, J.H., Friend, C.R.L., Hall, R.P., Jensen, S.B., Roberts, I.W.N., 1978. Continued 1: 500 000 reconnaissance mapping in the Precambrian of the Sukkertoppen region, southern West Greenland. Rapport Grønlands Geologiske Undersøgelse 90, 50–54.
- Arndt, N., 2013. Formation and Evolution of the Continental Crust. *Geochemical Perspectives* 2, 405–530.
- Arth, J.G., Barker, F., 1976. Rare-earth partitioning between hornblende and dacitic liquid and implications for the genesis of trondhjemitic-tonalitic magmas. *Geology* 4, 534–536.
- Berthelsen, A., 1962. Structural studies in the pre-Cambrian of western Greenland III. Southern Sukkertoppen district. Bulletin Grønlands Geologiske Undersøgelse 31, 46 pp.
- Berthelsen, A., Bridgwater, D., 1960. On the field occurrence and petrography of some basic dykes of supposed Pre-Cambrian age from the southern Sukkertoppen District, western Greenland. Bulletin Grønlands Geologiske Undersøgelse 24, 43 pp.
- Bizzarro, M., Simonetti, A., Stevenson, R.K., David, J., 2002. Hf isotope evidence for a hidden mantle reservoir. *Geology* 30, 771–774.
- Bridgwater, D., McGregor, V.R., Myers, J.S., 1974. A horizontal tectonic regime in the Archaean of Greenland and its implications for early crustal thickening. *Precambrian Research* 1, 179–197.
- Brown, M., Johnson, T., Gardiner, N.J., 2020. Plate tectonics and the Archean Earth. *Annual Review of Earth and Planetary Sciences* 48.
- Cawthorn, R.G., 2013. The Residual or Roof Zone of the Bushveld Complex, South Africa. *Journal of Petrology* 54, 1875–1900.
- Chadwick, B., Coe, K., 1988. Geologisk kort over Grønland. Grønlands Geologiske Undersøgelse, Nord, Copenhagen.
- Clark, D.A., 1999. Magnetic petrology of igneous intrusions: implications for exploration and magnetic interpretation. *Exploration Geophysics* 30, 5–26.

- Connelly, J.N., Mengel, F.C., 2000. Evolution of Archean components in the Paleoproterozoic Nagssugtoqidian orogen, West Greenland. *Geological Society of America Bulletin* 112, 747–763.
- Dyck, B., Reno, B.L., Kokfelt, T.F., 2015. The Majorqaaq Belt: a record of Neoproterozoic orogenesis during final assembly of the North Atlantic Craton, southern West Greenland. *Lithos* 220–223, 253–271.
- Friend, C.R.L., Nutman, A.P., 1994. Two Archean granulite-facies metamorphic events in the Nuuk-Maniitsoq region, southern West Greenland: correlation with the Saglek block, Labrador. *Journal of the Geological Society, London* 151, 421–424.
- Friend, C.R.L., Nutman, A.P., 2019. Tectono-stratigraphic terranes in Archean gneiss complexes as evidence for plate tectonics: The Nuuk region, southern West Greenland. *Gondwana Research* 72, 213–237.
- Friend, C.R.L., Nutman, A.P., McGregor, V.R., 1988. Late Archean terrane accretion in the Godthåb region, southern West Greenland. *Nature* 335, 535–538.
- Garde, A.A., 1987. *Geologisk kort over Grønland. Grønlands Geologiske Undersøgelse*, Copenhagen.
- Garde, A.A., 1989. *Geologisk kort over Grønland. Grønlands Geologiske Undersøgelse*, Nord, Copenhagen.
- Garde, A.A., 1990. Thermal granulite-facies metamorphism with diffuse retrogression in Archean orthogneisses, Fiskefjord, southern West Greenland. *Journal of Metamorphic Geology* 8, 663–682.
- Garde, A.A., 1991. Post-kinematic diorite intrusions in Archean basement rocks around outer Fiskefjord, southern West Greenland. *Bulletin of the Geological Society of Denmark* 39, 167–177.
- Garde, A.A., 1997. Accretion and evolution of an Archean high-grade grey gneiss-amphibolite complex: the Fiskefjord area, southern West Greenland. *Geology of Greenland Survey Bulletin* 177, 114.
- Garde, A.A., 2007. A mid-Archean island arc complex in the eastern Akia terrane, Godthåbsfjord, southern West Greenland. *Journal of the Geological Society* 164, 565–579.
- Garde, A.A., Dyck, B., Esbensen, K., Johansson, L., Möller, C., 2014. The Finnefeld domain, Maniitsoq structure, West Greenland: Differential rheological features and mechanical homogenisation in response to impacting? *Precambrian Research* 255, 791–808.
- Garde, A.A., Friend, C.R.L., Nutman, A.P., Marker, M., 2000. Rapid maturation and stabilisation of middle Archean continental crust: the Akia terrane, southern West Greenland. *Bulletin of the Geological Society of Denmark* 47, 1–27.
- Garde, A.A., Hall, R.P., Hughes, D.J., Jensen, S.B., Nutman, A.P., Stecher, O., 1983. Mapping of the Isukasia sheet, southern West Greenland. *Rapport Grønlands Geologiske Undersøgelse* 115, 20–29.
- Garde, A.A., Larsen, O., Nutman, A.P., 1986. Dating of late Archean crustal mobilisation north of Qugssuk, Godthåbsfjord, southern West Greenland. *Rapport Grønlands Geologiske Undersøgelse* 128, 23–36.
- Garde, A.A., McDonald, I., Dyck, B., Keulen, N., 2012a. Searching for giant, ancient impact structures on Earth: The Mesoproterozoic Maniitsoq structure, West Greenland. *Earth and Planetary Science Letters* 337–338, 197–210.
- Garde, A.A., Pattison, J., Kokfelt, T.F., McDonald, I., Secher, K., 2012b. The norite belt in the Mesoproterozoic Maniitsoq structure, southern West Greenland: conduit-type Ni-Cu mineralisation in impact-triggered, mantle-derived intrusions? *Geological Survey of Denmark and Greenland Bulletin* 28, 45–48.
- Garde, A.A., Whitehouse, M., Christensen, R., 2012c. Mesoproterozoic epithermal gold mineralisation preserved at upper amphibolite-facies grade, Qussuk, southern West Greenland. *Econ. Geol.* 107, 881–908.
- Gardiner, N.J., Kirkland, C.L., Hollis, J.A., Cawood, P.A., Nebel, O., Szilas, K., Yakymchuk, C., 2020. North Atlantic Craton architecture revealed by kimberlite-hosted crustal zircons. *Earth and Planetary Science Letters* 534, 116091.
- Gardiner, N.J., Kirkland, C.K., Hollis, J., Szilas, K., Steenfelt, A., Yakymchuk, C., Heide-Jørgensen, H., 2019. Building Mesoproterozoic crust upon Eoarchean roots: The Akia Terrane, West Greenland. *Contributions to Mineralogy and Petrology* 174, 1–20.
- Grant, F.S., 1985. Aeromagnetics, geology and ore environments. I. Magnetite in igneous, sedimentary and metamorphic rocks: an overview. *Geoexploration* 23, 303–333.
- Hall, R.P., 1984. Comparative geochemistry of Archean orthogneisses from the north-western quadrant of the Isukasia map sheet region, southern West Greenland. *Rapport Grønlands Geologiske Undersøgelse* 120, 37–45.
- Hall, R.P., Hughes, D.J., 1982. Transitional amphibolite-granulite facies granites, diorites and metalvolcanic amphibolites in the Isukasia map sheet, southern West Greenland. *Rapport Grønlands Geologiske Undersøgelse* 110, 46–49.
- Hall, R.P., Hughes, D.J., 1987. Noritic dykes of southern West Greenland: early Proterozoic boninitic magmatism. *Contributions to Mineralogy and Petrology* 97, 169–182.
- Halla, J., 2018. Highlights on Geochemical Changes in Archean Granitoids and Their Implications for Early Earth Geodynamics. *Geosciences* 8, geosciences8090353.
- Halla, J., Whitehouse, M.J., Ahmad, T., Bagai, Z., 2017. Archean granitoids: An overview and significance from a tectonic perspective. In: Halla, J., Whitehouse, M. J., Ahmad, T., Bagai, Z. (Eds.), *Crust-Mantle Interactions and Granitoid Diversification: Insights from Archean Cratons*. UK, Geological Society, London, pp. 1–18.
- Hanmer, S., Hamilton, M.A., Crowley, J.L., 2002. Geochronological constraints on Paleoproterozoic thrust-nappe and Neoproterozoic accretionary tectonics in southern West Greenland. *Tectonophysics* 350, 255–271.
- Hastie, A.R., Fitton, J.G., 2019. Eoarchean tectonics: New constraints from high pressure-temperature experiments and mass balance modelling. *Precambrian Research* 325, 20–38.
- Hawkesworth, C. J., Cawood, P. A., Dhuime, B. and Kemp T.I.S. 2017. Earth's Continental Lithosphere Through Time. *Annu. Rev. Earth Planet. Sci.* 45, 169–98.
- Henkel, H., 1991. Petrophysical properties (density and magnetization) of rocks from the northern part of the Baltic Shield. *Tectonophysics* 192, 1–19.
- Henkel, H., Eriksson, L., 1987. Regional aeromagnetic and gravity studies in Scandinavia. *Precambrian Research* 35, 169–180.
- Henkel, H., Guzmán, M., 1977. Magnetic features of fracture zones. *Geoexploration* 15, 173–181.
- Henriksen, N., Higgins, A. K., Kalsbeek, F., Pulvertaft, T. C. R. 2000. *Greenland from Archean to Quaternary. Descriptive text to the 1995 Geological map of Greenland 1:2 500 000. 2nd edition. Geological Survey of Denmark and Greenland Bulletin* 18, 126 pp.
- Hoffmann, J.E., Kröner, A., Hegner, E., Viehmann, S., Xie, H., Iaccherie, L.M., Schneider, K.P., Hofmann, A., Wong, J., Geng, H., Yang, J., 2016. Source composition, fractional crystallization and magma mixing processes in the 3.48–3.43 Ga Tsawela tonalite suite (Ancient Gneiss Complex, Swaziland) – Implications for Palaeoproterozoic geodynamics. *Precambrian Research* 276, 43–66.
- Hollis, J. A. (ed.) 2005. *Greenstone belts in the central Godthåbsfjord region, southern West Greenland: Geochemistry, geochronology and petrography arising from 2004 field work, and digital map data. Danmarks og Grønlands Geologiske Undersøgelse Rapport* 2005/42, 215 pp.
- Hollis, J.A., Frei, D., van Gool, J.A.M., Garde, A.A., Persson, M., 2006. Using zircon geochronology to resolve the Archean geology of southern West Greenland. *Geological Survey of Denmark and Greenland Bulletin* 10, 49–52.
- Jackson, S.E., Pearson, N.J., Griffin, W.L., Belousova, E.A., 2004. The application of laser ablation-inductively coupled plasma-mass spectrometry to in situ U/Pb zircon geochronology. *Chemical Geology* 211, 47–69.
- Jacobsen, B.H., 1987. A case for upward continuation as a standard separation filter for potential-field maps. *Geophysics* 52, 1138–1148.
- Kalsbeek, F., Garde, A.A., 1989. Geological map of Greenland 1:500 000. Descriptive text. Sheet 2. Frederikshåb Isblink - Sønder Strømfjord. *Grønlands Geologiske Undersøgelse*, Copenhagen.
- Käpyaho, A., 2006. Whole-rock geochemistry of some tonalite and high-Mg/Fe gabbro, diorite, and granodiorite plutons (sanukitoid suites) in the Kuhmo district, eastern Finland. *Bulletin of the Geological Society of Finland* 78, 121–141.
- Keulen, N., Garde, A.A., Jørgart, T., 2015. Shock melting of K-feldspar and interlocking with cataclastically deformed plagioclase in granitic rocks at Toqqusap Nunaa, southern West Greenland: Implications for the genesis of the Maniitsoq structure. *Tectonophysics* 662, 328–344.
- Kirkland, C. L., Hollis, J. and Gardiner, N. J. 2016. *Greenland U-Pb geochronology database.* <http://www.greenmin.gl/>.
- Kirkland, C. L., Olierook, H., Yakymchuk, C., Gardiner, N. J., Szilas, K. and Johnson, T. in review. Theoretical versus empirical secular change in Archean zircon composition. *Earth Planet. Sci. Lett.*
- Kirkland, C.L., Yakymchuk, C., Hollis, J., Heide-Jørgensen, H., Danišić, M., 2018. Mesoproterozoic exhumation of the Akia terrane and a common Neoproterozoic tectonothermal history for West Greenland. *Precambrian Research* 314, 129–144.
- Kirkland, C.L., Yakymchuk, C., Szilas, K., Evans, N., Hollis, J., McDonald, B., Gardiner, N. J., 2018. Apatite: a U–Pb thermochronometer or geochronometer? *Lithos* 318–319, 143–157.
- Knudsen, C., 1991. Geology and geochemistry of the Qaqarsuk carbonatite complex, southern West Greenland. In: Friedrich, G. (Ed.), *SGA, Monograph Series on Mineral Deposits* 29. Gebrüder Borntraeger, Berlin, p. 110.
- Larsen, H.C., 1981. A high-pressure granulite facies complex in north-west Payers Land, East Greenland fold belt. *Bulletin of the Geological Society of Denmark* 29, 161–174.
- Larsen, L.M., Heaman, L., Creaser, R.A., Duncan, R.A., Frei, R., Hutchison, M., 2009. Tectonomagmatic events during stretching and basin formation in the Labrador Sea and the Davis Strait: evidence from age and composition of Mesozoic to Palaeogene dyke swarms in West Greenland. *Journal of the Geological Society, London* 166, 999–1012.
- Larsen, L.M., Pedersen, A.K., 1982. A minor carbonatite occurrence in southern West Greenland: the Tupertalik intrusion. *Rapport Grønlands Geologiske Undersøgelse* 110, 38–43.
- Laurent, O., Björnsen, J., Wotzlaw, J.-F., Bretscher, S., Silva, M.P., Moya, J.-F., Ulmer, P., Bachmann, O., 2020. Earth's earliest granitoids are crystal-rich magma reservoirs tapped by silicic eruptions. *Nature Geoscience* 13, 163–169.
- Letts, S., Torsvik, T.H., Webb, S.J., Ashwal, L.D., 2011. New Palaeoproterozoic palaeomagnetic data from the Kaapvaal Craton, South Africa. *Geological Society, London, Special Publications* 357, 9–26.
- Martin, H., 1994. The Archean grey gneisses and the genesis of Archean crust. In: Condie, K.C. (Ed.), *Archean crustal evolution*. Elsevier, Amsterdam, pp. 205–259.
- Mayborn, K.R., Leshner, C.E., 2006. Origin and evolution of the Kangamiut mafic dyke swarm, West Greenland. *Geological Survey of Denmark and Greenland Bulletin* 11, 61–86.
- McGregor, V.R., 1984. *Geologisk kort over Grønland. Grønlands Geologiske Undersøgelse*, Copenhagen.
- McGregor, V. R. 1993. *Geological map of Greenland 1:100 000. Descriptive text. Qórut 64 V.1 Syd. The regional geology of part of the Archean block of southern West Greenland, including a segment of the late Archean mobile belt through Godthåbsfjord. Copenhagen: Grønlands Geologiske Undersøgelse.*
- McGregor, V.R., Friend, C.R.L., Nutman, A.P., 1991. The late Archean mobile belt through Godthåbsfjord, southern West Greenland: a continent-continent collision zone? *Bulletin of the Geological Society of Denmark* 39, 179–197.
- Moya, J.-F., 2011. The composite Archean grey gneisses: petrological significance, and evidence for a non-unique tectonic setting for Archean crustal growth. *Lithos* 123, 21–36.
- Moya, J.-F., Martin, H., 2012. Forty years of TTG research. *Lithos* 148, 312–336.

- Naeraa, T., Schersten, A., Rosing, M.T., Kemp, A.I., Hoffmann, J.E., Kokfelt, T.F., Whitehouse, M.J., 2012. Hafnium isotope evidence for a transition in the dynamics of continental growth 3.2 Gyr ago. *Nature*, London 485, 627–630.
- Nielsen, B. M., Rasmussen, T. M. 2004. Mineral resources of the Precambrian shield of central West Greenland (66° to 70°15'N). Part 3. Implications of potential field data for the tectonic framework. *Danmarks og Grønlands Geologiske Undersøgelse Rapport 2004/21*, 141 pp.
- Nielsen, T.F.D., Jensen, S.M., Secher, K., Sand, K.K., 2009. Distribution of kimberlite and allikite in the Diamond Province of southern West Greenland: A regional perspective based on groundmass mineral chemistry and bulk compositions. *Lithos* 112 (Supplement), 358–437.
- Nilsson, M.K.M., Klausen, M.B., Söderlund, U., Ernst, R.E., 2013. Precise U-Pb ages and geochemistry of Palaeoproterozoic mafic dykes from southern West Greenland: Linking the North Atlantic and the Dharwar cratons. *Lithos* 255–270.
- Nilsson, M.K.M., Söderlund, U., Ernst, R.E., Hamilton, M.A., Scherstén, A., Armitage, P.E. B., 2010. Precise U-Pb baddeleyite ages of mafic dykes and intrusions in southern West Greenland and implications for a possible reconstruction with the Superior craton. *Precambrian Research* 183, 399–415.
- Noe-Nygaard, A., Ramberg, H., 1961. Geological reconnaissance map of the country between latitudes 69°N and 63°45'N. West Greenland. *Meddelelser om Grønland* 123, 9 pp.
- Nutman, A.P., Bennett, V.C., Friend, C.R.L., Yi, K., Lee, S.R., 2015. Mesoarchaean collision of Kapisilik terrane 3070Ma juvenile arc rocks and >3600Ma Isukasia terrane continental crust (Greenland). *Precambrian Research* 258, 146–160.
- Nutman, A.P., Friend, C.R.L., Baadsgaard, H., McGregor, V.R., 1989. Evolution and assembly of Archean gneiss terranes in the Godthåbsfjord region, southern West Greenland: structural, metamorphic, and isotopic evidence. *Tectonics* 8, 573–589.
- Nutman, A. P., Friend, C. R. L., Barker, S. L. L., McGregor, V. R. 2004. Inventory and assessment of Palaeoarchaean gneiss terrains and detrital zircons in southern West Greenland. In: S. J. Mojzsis (Ed.) *The first billion years: selected papers presented at the 13th V.M.Goldschmidt conference* 135. *Precambrian Research*. 281-314.
- Nutman, A.P., Hagiya, H., Maruyama, S., 1995. SHRIMP U-Pb single zircon geochronology of a Proterozoic mafic dyke, Isukasia, southern West Greenland. *Bull. Geol. Soc. Den.* 42, 17–22.
- Nutman, A.P., Kalsbeek, F., Marker, M., van Gool, J.A.M., Bridgwater, D., 1999. U-Pb zircon ages of Kangamiut dykes and detrital zircons in metasediments in the Palaeoproterozoic Nagssugtoqidian Orogen (West Greenland). Clues to the pre-collisional history of the orogen. *Precambrian Research* 93, 87–104.
- Olesen, O., Henkel, H., Kaada, K., Tveten, E., 1991. Petrophysical properties of a prograde amphibolite-granulite facies transition zone at Sigerfjord, Vesterålen, northern Norway. *Tectonophysics* 192, 33–39.
- Olierook, H.K.H., Kirkland, C.L., Szilas, K., Hollis, J., Gardiner, N., Steenfelt, A., 2020. Cryptic zircon inheritance: the need for comprehensive mapping, sampling and chemical data in the interpretation of U-Pb geochronology. *Journal of Petrology*.
- Ontario Geological Survey 2001. Physical rock property data from the Physical Rock Property Study in the Timmins and Kirkland Lake Areas; Ontario Geological Survey, Miscellaneous Release – Data 91.
- Palin, R.M., Santosh, M., Cao, W., Li, S.S., Hernández-Urbe, D., Parsons, A., 2020. Secular metamorphic change and the onset of plate tectonics. *Earth Sci. Rev.*
- Paton, C., Hellstrom, J., Paul, B., Woodhead, J., Hergt, J., 2011. Iolite: freeware for the visualization and processing of mass spectrometer data. *Journal of Analytical Atomic Spectrometry* 26, 2508–2518.
- Polat, A., Wang, L., Appel, P.W.U., 2015. A review of structural patterns and melting processes in the Archean craton of West Greenland: Evidence for crustal growth at convergent plate margins as opposed to non-uniformitarian models. *Tectonophysics* 662, 67–94.
- Poulsen, V., 1966. An occurrence of Lower Palaeozoic rocks within the Precambrian terrain near Sukkertoppen. *Rapport Grønlands Geologiske Undersøgelse* 11, 26 only.
- Puranen, R., 1989. Susceptibilities, iron and magnetite content of Precambrian rocks in Finland. *Geological Survey of Finland, Report of Investigation* 90, 1–45.
- Rasmussen, T.M., Thorning, L., 1999. Airborne geophysical surveys in Greenland in 1998. *Geology of Greenland Survey Bulletin* 183, 34–38.
- Ravenelle, J.-F., Weiershäuser, L., 2017. Updated independent technical report for the Maniitsoq nickel-copper-cobalt-PGM project, Greenland. North American Nickel website. North American Nickel website [www.northamericannickel.com](http://www.northamericannickel.com), 187 pp.
- Reimold, W. U., Gibson, R. L., Koerber, C. 2013. Comment on “Searching for giant, ancient impact structures on Earth: The Mesoarchaean Maniitsoq structure, West Greenland” by Garde et al. [*Earth Planet. Sci. Lett.* 337-338 (2012) 197-210]. *Earth Planet. Sci. Lett.* 369-370, 333-335.
- Reimold, W.U., Ferriere, L., Deutsch, A., Koerber, C., 2014. Impact controversies: Impact recognition criteria and related issues. *Meteoritics & Planetary Science* 49, 723–731.
- Riciputi, L.R., Valley, J.W., McGregor, V.R., 1990. Conditions of Archean granulite metamorphism in the Godthåb-Fiskenaeset region, southern West Greenland. *Journal of Metamorphic Geology* 8, 171–190.
- Rosing, M.T., Nutman, A.P., Løfqvist, L., 2001. A new fragment of the early earth crust: the Aasivik terrane of West Greenland. *Precambrian Research* 105, 115–128.
- Rudnick, R.L., Gao, S., 2014. 4.1 - Composition of the Continental Crust. In: *Treatise on Geochemistry* (Second Edition). Elsevier, pp. 1–51.
- Sandrin, A., Elming, S.-Å., 2006. Geophysical and petrophysical study of an iron oxide copper gold deposit in northern Sweden. *Ore Geology Reviews* 29, 1–18.
- Sandrin, A., Berggren, R., Elming, S.-Å., 2007. Geophysical targeting of Fe-oxide Cu-(Au) deposits west of Kiruna, Sweden. *J. Appl. Geoph.* 61, 92–101.
- Scherstén, A., Garde, A.A., 2013. Complete hydrothermal re-equilibration of zircon in the Maniitsoq structure, West Greenland: A 3001 Ma minimum age of impact? *Meteoritics and Planetary Science* 48, 1472–1498.
- Secher, K., 1983. Noritic rocks and associated nickel-copper-sulphide occurrences in Sukkertoppen district, central West Greenland. *Rapport Grønlands Geologiske Undersøgelse* 115, 30–34.
- Sláma, J., Köslér, J., Condon, D.J., Crowley, J.L., Gerdes, A., Hanchar, J.M., Horstwood, M.S.A., Morris, G.A., Nasdala, L., Norberg, N., Schaltegger, U., Schoene, B., Tubrett, M.N., Whitehouse, M.J., 2008. Plešovice zircon - a new natural reference material for U-Pb and Hf isotopic microanalysis. *Chemical Geology* 249, 1–35.
- Stacey, J.S., Kramers, J.D., 1975. Approximation of terrestrial lead isotope evolution by a two-stage model. *Earth and Planetary Science Letters* 26, 207–221.
- Steenfelt, A., 1987. Geochemical mapping and prospecting in Greenland - a review of results and experience. *Journal of Geochemical Exploration* 29, 183–205.
- Steenfelt, A., 1999. Compilation of data sets for a geochemical atlas of West and South Greenland based on stream sediment surveys 1977 to 1997. *Danmarks og Grønlands Geologiske Undersøgelse Rapport 1999 (41)*, 33.
- Steenfelt, A. 2001. Geochemical atlas of Greenland – West and South Greenland. *Danmarks og Grønlands Geologiske Undersøgelse Rapport 2001/46*, 39 pp.
- Steenfelt, A., 2012. Rare earth elements in Greenland: known and new targets identified and characterised by regional stream sediment data. *Geochemistry: Exploration, Environment, Analysis* 12, 313–326.
- Steenfelt, A., Garde, A.A., Moyén, J.-F., 2005a. Mantle wedge involvement in the petrogenesis of Archean grey gneisses in West Greenland. *Lithos* 79, 207–228.
- Steenfelt, A., Jensen, S.M., Nielsen, T.F.D., Sand, K.K., Secher, K., 2009. Diamonds and lithospheric mantle properties in the Neoproterozoic igneous province of southern West Greenland. *Geological Survey of Denmark and Greenland Bulletin* 17, 65–68.
- Steenfelt, A., Moberg, E., Schjøth, F. 2005. Use of stream sediment and lithological data to estimate the chemical compositions of three land areas in South Greenland. *Danmarks og Grønlands Geologiske Undersøgelse Rapport 2005/39*, 52 pp.
- Stern, R. A. 2001. A new isotopic and trace-element standard for the ion microprobe: preliminary thermal ionization mass spectrometry (TIMS) U-Pb and electron-microprobe data. *Geological Survey of Canada, Radiogenic Age and Isotopic Studies, Report 14, Current Research 2001-F1*, 11p.
- Stern, R.A., Bodorkos, S., Kamo, S.L., Hickman, A.H., Corfu, F., 2009. Measurement of SIMS Instrumental Mass Fractionation of Pb Isotopes During Zircon Dating. *Geostand. Geoanal. Res.* 33, 145–168.
- Stouge, S., Peel, J.S., 1979. Ordovician conodonts from the Precambrian Shield of southern West Greenland. *Rapport Grønlands Geologiske Undersøgelse* 91, 105–109.
- Szilas, K., Kelemen, P.B., Bernstein, S., 2015. Peridotite enclaves hosted by Mesoarchaean TTG-suite orthogneisses in the Fiskefjord region of southern West Greenland. *GeoResJ* 7, 22–34.
- Szilas, K., Tusch, J., Hoffmann, J.E., Garde, A.A., Münker, C., 2017. Hafnium isotope constraints on the origin of Mesoarchaean andesites in southern West Greenland, North Atlantic craton. *Geological Society, London, Special Publications* 449, 19–38.
- Szilas, K., van Hinsberg, V., McDonald, I., Næraa, T., Rollinson, H., Adetunji, J., Bird, D., 2018. Highly refractory Archean peridotite cumulates: Petrology and geochemistry of the Seqi Ultramafic Complex, SW Greenland. *Geoscience Frontiers* 9, 689–714.
- Tappe, S., Pearson, D.G., Nowell, G.M., Nielsen, T.F.D., Milstead, P., Muehlenbachs, K., 2011. A fresh isotopic look at Greenland kimberlites: cratonic mantle lithosphere imprint on deep source signal. *Earth Planet. Sci. Lett.* 305, 235–248.
- Tappe, S., Romer, R.L., Stracke, A., Steenfelt, A., Smart, K.A., Muehlenbachs, K., Torsvik, H., 2017. Sources and mobility of carbonate melts beneath cratons, with implications for deep carbon cycling, metasomatism and rift initiation. *Earth and Planetary Science Letters* 466, 152–167.
- van Gool, J.A.M., Connelly, J.N., Marker, M., Mengel, F., 2001. The Nagssugtoqidian Orogen of West Greenland: tectonic evolution and regional correlations from a West Greenland perspective. *Canadian Journal of Earth Sciences* 39, 665–686.
- Verduzco, B., Fairhead, J.D., Green, C.M., MacKenzie, C., 2004. New insights into magnetic derivatives for structural mapping. *The Leading Edge* 23, 116–119.
- Waterton, P., Hyde, W. R., Tusch, J., Hollis, J. A., Kirkland, C. L., Kinney, C., Yakymchuk, C., Gardiner, N. J., Zakharov, D., Olierook, H., Münker, C., Lightfoot, P. C. and Szilas, K. in review. Geodynamic implications of synchronous norite and TTG formation in the 3 Ga Maniitsoq Norite Belt, West Greenland. *Frontiers in Earth Science*.
- White, R.W., Palin, R.M., Green, E.C., 2017. High-grade metamorphism and partial melting in Archean composite grey gneiss complexes. *J. Metamorph. Geol.* 35, 181–195.
- Wiedenbeck, M., Allé, P., Corfu, F., Griffin, W.L., Meier, M., Oberli, F., von Quadt, A., Roddick, J.C., Spiegel, W., 1995. Three natural zircon standards for U-Th-Pb, Lu-Hf, trace element and REE analyses. *Geostandards Newsletter* 19, 1–23.
- Windle, B.F., Garde, A.A., 2009. Arc-generated blocks with crustal sections in the North Atlantic craton of West Greenland: Crustal growth in the Archean with modern analogues. *Earth-Science Reviews* 93, 1–30.
- Wingate, M.T.D., Kirkland, C.L., 2015. Introduction to geochronology information released in 2015. *Geological Survey of Western Australia* 5p.
- Yakymchuk, C., Kirkland, C. L., Hollis, J. A., Kendrick, J., Gardiner, N., Szilas, K. 2020. Reworking of Mesoarchaean crust during high-temperature-low-pressure metamorphism, Akia terrane, west Greenland. *Precambrian Research* in review.
- Yi, K., Bennett, V.C., Nutman, A.P., Lee, S.R., 2014. Tracing Archean terranes under Greenland's Icecap: U-Th-Pb-Hf isotopic study of zircons from melt-water rivers in the Isua area. *Precambrian Research* 255, 900–921.